This is a preprint, the final version is subject to change, of the American Mineralogist (MSA)
Cite as Authors (Year) Title. American Mineralogist, in press.
(DOI will not work until issue is live.) DOI: http://dx.doi.org/10.2138/am.2014.4540

Weathering of cobalt arsenides: natural assemblages and calculated stability relations among secondary Ca-Mg-Co arsenates and carbonates

REVISION 1

Gregor Markl*, [1], Michael A. W. Marks[1], Insa Derrey[1,2], Jan-Erik Gühring[1]

1 = Fachbereich Geowissenschaften, Universität Tübingen, Wilhelmstr. 56, D-72074 Tübingen, Germany

2 = Institut für Mineralogie, Leibniz Universität Hannover, Callinstr. 3, D-30167 Hannover, Germany.

* = corresponding author; markl@uni-tuebingen.de

This is a preprint, the final version is subject to change, of the American Mineralogist (MSA)
Cite as Authors (Year) Title. American Mineralogist, in press.
(DOI will not work until issue is live.) DOI: http://dx.doi.org/10.2138/am.2014.4540

Abstract

The supergene alteration of cobalt arsenides produces a variety of characteristic mineral assemblages including erythrite, pharmacolite and other Ca±Mg±Co-bearing arsenates, which upon precipitation remove Co and As from natural waters. Their paragenetic relationships and stability conditions have not been investigated in detail. We present a detailed study on these assemblages, their successions and coexisting fluid compositions from the mining area of Wittichen, SW Germany, where primary skutterudite and safflorite in granite-hosted barite-calcite veins are undergoing oxidation. Water analyses from the old mines, a semi-quantitative stability diagram and quantitative reaction path modeling are used to constrain their conditions of formation.

Cobalt- and arsenate-bearing solutions invariably precipitate erythrite first and hence buffer Co concentrations to very low values. Both during skutterudite or safflorite dissolution and erythrite precipitation, the fluid's Co/As ratio decreases rapidly. Therefore, spherocobaltite (Co carbonate) is unstable in the presence of arsenate ions under most conditions.

The formation of various mineral assemblages precipitating after or simultaneously with erythrite strongly depends on Ca^{2+} and Mg^{2+} activities and pH. Small changes in one of these parameters lead to different mineral assemblages. These small changes are partly governed by fluid-host rock or fluid-vein mineral reactions and partly by the precipitation of the secondary arsenate minerals themselves. This complex interdependence produces the rich variety of mineral assemblages observed, which effectively serves as a very sensitive monitor of fluid compositions. Furthermore, the assemblages themselves are able to buffer the Ca-Mg-Co-As concentrations in the fluid to some extent and effectively immobilize both As and Co in close proximity to the ore deposit.

Keywords: cobalt, arsenate, weathering, erythrite, pharmacolite, spherocobaltite, phase stabilities, reaction path modeling

This is a preprint, the final version is subject to change, of the American Mineralogist (MSA)
Cite as Authors (Year) Title. American Mineralogist, in press.
(DOI will not work until issue is live.) DOI: http://dx.doi.org/10.2138/am.2014.4540

Introduction

Cobalt is an important high-tech metal, which is gained primarily as by- or co-product from lateritic or hydrothermal Co-Ag mineralizations and "Five-element veins": Cobalt-Gowganda, Ontario/Canada, Erzgebirge and Richelsdorfer Gebirge in Central Europe, Kongsberg and Modum/Norway, Bou Azzer, Morocco; Co-Cu mineralizations: Katanga, Democratic Republic of Kongo (e.g., Dill, 2010; Lefebure, 1996; Gervilla et al., 2012) or metamorphic/metasomatic deposits: Black Bird District, Idaho; NICO, NWT/Canada; Haarakumpu, Finland; Skutterud, Norway (e.g., Slack et al., 2010). The principal non-oxide ore minerals mined for cobalt are sulfides like carrollite ($Cu(Co, Ni)_2S_4$) or cobaltpentlandite ($(Co,Ni,Fe)_9S_8$), sulfarsenides like cobaltite (CoAsS) or arsenides like safflorite ($(Co, Fe, Ni)As_2$), and skutterudite ($(Co, Fe, Ni)As_{2-3}$).

Weathering of ore deposits containing the above minerals potentially release significant amounts of heavy metals, especially of Co, Ni and As. These partially toxic elements can either reach the groundwater or be (partly?) fixed in or adsorbed to newly formed supergene mineral phases (e.g. for Co: erythrite or Co-bearing oxide/hydroxide minerals such as asbolane and heterogenite; Brown & Calas, 2012). Accordingly, it is important to know exactly the supergene mineralogy developing in and around such ore deposits to be able to judge the environmental impact of both natural weathering and anthropogenic heap leaching (e.g. Dold & Fontboté, 2001; Álvarez-Valero et al., 2008; Valente & Gomes, 2009; Dold et al., 2009). While Co-Ni-Fe-bearing sulfides weather to produce various water-soluble sulfates (among which bieberite, the Co sulfate, is a very rare species) and hence are potentially hazardous to their environment, the oxidation of arsenides or sulfarsenides releases arsenate ions which lead - depending on other ions like Ca, Mg or Fe in the weathering solution - to the formation of abundant secondary arsenates, the most common and important being erythrite ($Co_3(AsO_4)_2*8H_2O$). Other species potentially occurring with erythrite are pharmacolite, picropharmacolite and a large variety of other Ca-Mg-Co arsenates listed in **table 1**. Interestingly, the association of erythrite with calcite is much more common than the occurrence of the Co carbonate spherocobaltite which is only known from few localities world-wide, and which only in Bou Azzer (Morocco) and Katanga (Democratic Republic of Kongo; e. g. from the Kakanda mine) occurs in larger quantities and cm-sized crystals (Fay & Barton, 2012).

Our knowledge about the stability relations among these secondary minerals, their paragenetic associations, the composition of coexisting fluids and their potential importance for the fixation of heavy metals is very poor. The few mineralogical

This is a preprint, the final version is subject to change, of the American Mineralogist (MSA)
Cite as Authors (Year) Title. American Mineralogist, in press.
(DOI will not work until issue is live.) DOI: http://dx.doi.org/10.2138/am.2014.4540

publications concerning such mineral associations mainly deal with their systematic mineralogy without reporting much information about their paragenetic associations (e. g. Juillot et al., 1999; Pierrot 1964; Walenta, 1972). The present contribution describes supergene mineral assemblages and fluid compositions found in a classic Co mining district of southern Germany, Wittichen near Schiltach, and presents results of PHREEQC modeling to understand the formation and evolution of such assemblages on a quantitative basis.

Geological Setting

The samples used in the present study come from old mines in the area of Wittichen in the Central Schwarzwald, SW Germany **(Fig. 1)**. This mining district has been mined at least since about 1300 for silver; between 1700 and about 1850, Co was the most important product used for blue color at that time (Markl, 2005). About 30 hydrothermal veins around the former monastery of Wittichen cut through the Triberg granite complex, a Variscan peraluminous two-mica granite, and the overlying quartzitic to arkosic sediments, which locally contain high amounts of dolomitic carbonate and carneol formed in a Permian paleo-soil environment (Martins & Pfefferkorn, 1988; Staude et al. 2012a). The veins consist of an early (Jurassic) association of pitchblende, native silver and bismuth with the cobalt and nickel arsenides safflorite, skutterudite and nickeline in a gangue of barite with minor calcite and quartz (Staude et al., 2012b). A later (probably Tertiary) mineralization phase precipitated Cu-Bi ores (wittichenite and emplectite) with another generation of barite and some fluorite (Staude et al., 2012b). Secondary minerals formed under supergene, oxidizing conditions and have been investigated in great detail (e. g., Waltena 1992 and references therein). Wittichen is the type locality for a number of these minerals, including orthowalpurgite, heinrichite, meta-novacekite, pharmacolite, meta-kirchheimerite and others (Markl & Slotta, 2011).

Oxidation of the primary ores occurred in three different environments:

1. in veins prior to human interference;
2. in veins exposed to water and air in the old adits and shafts during and after human interference;
3. in mine dumps after the mining ceased.

Here, we will only investigate the second case, which has, however, implications for the others as well.

This is a preprint, the final version is subject to change, of the American Mineralogist (MSA)
Cite as Authors (Year) Title. American Mineralogist, in press.
(DOI will not work until issue is live.) DOI: http://dx.doi.org/10.2138/am.2014.4540

Samples and analytical techniques

Mineral samples were collected in the following old mines (see Vogelgesang, 1865; Markl, 2005 and Staude et al., 2012b for precise locations of these mines in the area of Wittichen): Anton im Heubach, Sophia im Böckelsbach, St. Joseph, Neuglück/Simson, Johann Georg im Böckelsbach, Frisch Glück lower level and Johann am Burgfelsen. Most mineral samples were collected by various hobby collectors about 20 years ago when the mines were still open and accessible to the public; fluid samples were collected from the closed mines in 2011 with permission of the owner, Fürst zu Fürstenberg. In total, 98 mineral samples were investigated in detail by optical microscopy, X-ray diffraction (XRD) and electron microprobe (EMP). They consisted typically of hand-sized granite samples with or without barite-calcite-safflorite-skutterudite vein material overgrown by various associations of secondary minerals. Examples of the samples are shown in **Fig. 2**, the observed mineral associations at Wittichen (from this work) and at other central European occurrences (from the literature) are reported in **table 2**; the sequence of mineral assemblages observed on each investigated sample is presented in **electronic supplement A**. As the primary mineralization in all investigated mines is identical, the secondary phase assemblages do not depend on the mine they come from, but rather on the precise locality within a specific mine and the primary phase assemblage found there (e. g., with or without calcite; grown on top of vein material or on the host granite). The minerals were investigated first by a normal binocular and, when in doubt, small (around 1 mm^3) grains were retrieved from the samples to be analyzed by XRD and, if necessary, by energy-dispersive methods in the electron microprobe. Thus, all phases could be precisely determined.

Fluid samples were taken from 18 abandoned mines (Emanuel im Hengstbach, Alte Gabe Gottes in der Reinerzau, Daniel im Gallenbach, Georg am Burgfelsen, Dreikönigstern, Johann am Burgfelsen, Michael im Rohrbächle, Hilfe Gottes im Stammelbach, Maria Magdalena im Erdlinsbach, Güte Gottes in Hinterwittichen, Frisch Glück am Silberberg, Johann Georg im Böckelsbach, Löw-Leostollen, Anton von Padua am Burgfelsen, Katharina im Trillengrund, Erzwäschestollen am Hohberg, Flussspatgrube Reinerzau and Herzog Friedrich in der Reinerzau) using PET bottles (when fluid flow was sufficient) or syringes (when fluid availability was limited to few drops on mine walls). The latter were stored in Eppendorf safe lock tubes. Bottles and safe lock tubes were cleaned with acid and triply deionized water prior to sampling, according to the method described in Göb et al. (2013). Where possible, large samples

This is a preprint, the final version is subject to change, of the American Mineralogist (MSA)
Cite as Authors (Year) Title. American Mineralogist, in press.
(DOI will not work until issue is live.) DOI: http://dx.doi.org/10.2138/am.2014.4540

on the order of 1-2 l were taken (henceforth called macrosamples, MA). Drop samples and samples taken with syringes (henceforth called microsamples, MI) were on the order of 60 ml and 1.5 ml, respectively. Altogether 64 fluid samples were analyzed by ion chromatography (IC) and total reflection X-ray fluorescence spectroscopy (TXRF). Examples of the sampling sites of water samples are shown in **Fig. 3**.

Temperature, pH, specific conductivity and alkalinity of macrosamples were determined at the sampling site. Subsequently, all samples were filtered through a 0.2 µm cellulose acetate filter, acidified to pH = 2 to prevent any precipitation and stored cool (8°C) until further analysis.

Major anions (F^-, Cl^-, Br^-, NO_3^-, PO_4^{3-} and SO_4^{2-}) and cations (Li^+, Na^+, K^+, Mg^{2+}, Ca^{2+} and Ba^{2+}) were determined by ion chromatography (Dionex ICS-1000) at the Universität Tübingen, Fachbereich Geowissenschaften. Based on routine standard measurements, errors for major anions and cations are generally <10 %.

Other trace elements were analyzed at the Institut für Mineralogie und Geochemie, Karlsruhe, using a high-resolution ICP-MS instrument (VG Elemental). Analytical precision for trace elements is, based on standard analyses, better than 3%; for Si, Al and Fe, precision is better than 6%.

Samples with a volume smaller than that required for ICP-MS analysis (=30ml), were analyzed by TXRF. In this case, 990 µl of sample was thoroughly mixed with 10 µl of internal standard (10 mg/l Ga solution). Subsequently, three aliquots (each 10 µl) of this mixture were put onto polished quartz-discs, dried down and analyzed with a S2 PICOFOX benchtop TXRF system from Bruker AS equipped with a Mo X-ray tube, which was operated at 50 kV and 600 µA. The accuracy and reproducibility of the data were tested by repeatedly analyzing standard reference material NIST1643c (trace elements in water). For most elements the deviation from the target values were below 15 % relative. The pH-values, TDS, conductivity and concentration data for Ca, Mg, Co, Ni and As of the studied water samples are given in **table 3**, all major and minor element data for all fluid samples are given in the **electronic supplement B**.

Results

Mineral assemblages

The magmatic phase assemblage of the host rock granite consists of biotite, muscovite, K-feldspar, quartz and plagioclase with apatite, tourmaline and zircon as main accessories. Both biotite and plagioclase are hydrothermally altered to various extent

This is a preprint, the final version is subject to change, of the American Mineralogist (MSA)
Cite as Authors (Year) Title. American Mineralogist, in press.
(DOI will not work until issue is live.) DOI: http://dx.doi.org/10.2138/am.2014.4540

and show formation of mainly illite (both phases) and hematite (biotite only), rarely also of calcite and barite (plagioclase only) or chlorite (biotite only). K-feldspar is basically devoid of any alteration feature, while plagioclase is almost completely consumed. This alteration, however, has nothing to do with the supergene processes investigated here, but is a Jurassic hydrothermal overprint related to the formation of the primary vein assemblage (Staude et al., 2012b; Brockamp et al., 1998). It is, nonetheless, important to understand the geochemical composition of the supergene fluids, which are in equilibrium with a variously altered granite.

The mineral assemblages reported in **table 2** and in **electronic supplement A** require some introductory comments. Erythrite forms a solid solution series with both annabergite (Ni, however, is very subordinate in the Wittichen area) and hörnesite. Erythrite-hörnesite solid solutions are easily recognized based on their progressively lighter color: pure erythrite is of a dark pinkish violet and continuously changes its color via pink, light pink and a pinkish white to white which is the color of pure hörnesite. Qualitative tests with the EMP have confirmed this relation. Rauenthalite and phaunouxite are in most cases intimately intergrown and very fine-grained, so that a precise determination of these polymorphs was impossible. Therefore, they are always reported as rauenthalite/phaunouxite. The various Ca-Mg arsenate and carbonate phases incorporate Co to various extents, discernible by various shades of pink in various aggregates **(Fig. 2).** They have not been quantitatively analyzed.

In terms of mineral paragenetic relationships, it is obvious that erythrite is always the first mineral to form, either alone or in association with other Ca-Mg arsenates. In contrast, picropharmacolite is typically a late phase, as is calcite or monohydrocalcite (the latter being observed only very rarely). Spherocobaltite has not been observed at all, pharmacolite and picropharmacolite are next to erythrite clearly the most abundant supergene arsenates in these assemblages. Gypsum is a common member of the investigated assemblages. In dry air, i. e. in collections, pharmacolite may decompose to weilite (see e. g. Waltena, 1992 and references therein). Where observed, this is specifically noted in the **electronic supplement A**.

Finally, it has to be noted that the interpretation of two minerals growing next to each other in these low-temperature fluid-saturated systems as formed in equilibrium may not be strictly true, but this is the best we can do to deduce any conclusion.

Mine water compositions

This is a preprint, the final version is subject to change, of the American Mineralogist (MSA)
Cite as Authors (Year) Title. American Mineralogist, in press.
(DOI will not work until issue is live.) DOI: http://dx.doi.org/10.2138/am.2014.4540

The collected water samples had temperatures between 8.8 and 13.6 °C, variable but low conductivities between <50 and >500 µS/cm and pH-values between 6 and 8.3 with no clear differences between waters in contact with the country rock granite, the gangue minerals or sinters **(Table 3 & Fig. 4a)**. Except for two outliers, all waters belong to the Ca-HCO_3-type, with relatively low Na, K, Cl and SO_4 concentrations (typically below 10 mg/l; **Table 3; Fig. 4b**), similar to other mine waters from the Schwarzwald (Göb et al., 2013). Mg, however, is an important cation in some of the waters (up to 28 mg/l) and clearly correlates with Ca (**Fig. 5A**). Co, Ni and As concentrations are highly variable and are correlated with each other (**Table 3; Fig. 5**). They range over several orders of magnitude depending on the type of water sample. Especially some of the sinter waters reach exceptionally high concentrations of Co (up to 75 µg/l), Ni (up to 240 µg/l) and As (up to 10800 µg/l).

Discussion

Occurrence of Ca-Mg-Co arsenates

Erythrite and Ca-Mg arsenates like pharmacolite and picropharmacolite have probably been known to miners for thousands of years; Hlousek & Tvrdy (2002) state that they have been used by old miners as indicators of ore mineralization. The first formal description as a mineral, however, was not until 1800, when Selb (1800) described and Karsten (1800) named pharmacolite from the Wittichen area. Since then, a total of 18 mineral species in the system Ca-Mg-As has been described and IMA-approved **(Fig. 6),** not to mention related species containing Co, phosphate or sulfate.

Because of their long mining and mineralogical tradition, several central European localities are the best investigated ones concerning their supergene Ca-Mg-Co arsenates: Schneeberg in the Saxonian part of the Erzgebirge (Germany), Jachymov (former Joachimsthal) in the Czech part of the Erzgebirge, St. Marie-aux-Mines in the Vosges Mountains of France, Richelsdorf in Thuringia (Germany) and Wittichen in the Schwarzwald, Germany (Bari, 1983; Hlousek & Tvrdy, 2002; Tvrdy & Karlovy, 2002; Massanek & Michalski, 2005; Schnorrer-Köhler, 1983; Walenta, 1972; 1987; 1992; Walenta & Dunn, 1989).

The formation of Ca-Mg-Co arsenates can occur by three different processes characterized by three different appearances of these minerals:

1. Interaction of a Co arsenide with an oxidizing meteoric fluid leads to a pH decrease of the fluid during As oxidation, which moves on and later reacts with a vein carbonate

This is a preprint, the final version is subject to change, of the American Mineralogist (MSA)
Cite as Authors (Year) Title. American Mineralogist, in press.
(DOI will not work until issue is live.) DOI: http://dx.doi.org/10.2138/am.2014.4540

(calcite or dolomite). pH increase and increase in Ca and/or Mg result in precipitation of erythrite and Ca-Mg arsenates.

2. Interaction of a meteoric fluid with calcite, dolomite or relict plagioclase in the host granite. In this case, the fluid's pH increases due to carbonate or plagioclase dissolution. Subsequently, if it comes in contact with Co arsenides, it dissolves them and precipitates erythrite and Ca-Mg arsenates due to the increase of arsenate activity.

3. Mixing of the fluids from the first two scenarios on a fracture in the absence of carbonates or arsenides.

All three cases occur in Wittichen, as proven by the textures shown in **Fig. 2:** Ca-Mg arsenates occur on calcite/dolomite veins **(case 1, Fig. 2A),** on Co arsenide veins (case 2, **Fig. 2B**) and on unmineralized fractures of the host granite (case 3, **Fig. 2C**).

Paragenetic relationships

The observed associations of Ca-Mg arsenates with each other and with erythrite, calcite and gypsum are reported in **table 2** and in **electronic supplement A. Table 2** additionally reports observations from the literature from the four Central European mining areas introduced above. We explicitly state, however, that these publications did not make a special effort to describe stable paragenetic relationships and we therefore tried to deduce equilibrium assemblages from their descriptions. We admit that based on the textures (and especially on the literature descriptions) alone, it is very difficult to decide if true thermodynamic equilibrium prevailed during their formation, and for example, the common intergrowth of the two polymorphs rauenthalite and phaunouxite may indicate disequilibrium textures. However, the fact that some associations and especially some sequences of specific associations are observed in many cases or even on almost all samples (e. g., the common occurrence of erythrite as the earliest phase) supports the decision to discuss the observed associations by means of equilibrium thermodynamics.

Figure 7 shows an activity-activity diagram in the Ca-Mg-As system, which was constructed semi-quantitatively using the slope of the respective reactions (based on their stoichiometry). We made the assumption of pure water and that As is present in excess. This means, the reaction stoichiometries were balanced based on As such as the following example:

$$2\ Mg_3(AsO_4)_2{*}8H_2O + 4\ Ca^{2+} + 2H^{+} = Ca_4Mg(AsO_3OH)_2(AsO_4)_2{*}11H_2O + 5\ Mg^{2+} + 5\ H_2O \quad \text{(Eq. 1)}$$

hörnesite picropharmacolite

This is a preprint, the final version is subject to change, of the American Mineralogist (MSA)
Cite as Authors (Year) Title. American Mineralogist, in press.
(DOI will not work until issue is live.) DOI: http://dx.doi.org/10.2138/am.2014.4540

The diagram shows the "parageneses" reported in **table 2**. The concentrations of Ca and Mg in fluids in equilibrium with a granitic host rock as well as their pH values are relatively well known (z. B. Göb et al., 2013; Bucher & Stober, 2010). In addition, our water analyses reported in **Table 3** and in the **electronic supplement** B allow to constrain these parameters even better. Given these analyses and the observed mineral associations at Wittichen (**Table 2**), it is possible to quantify the diagram of Fig. 10 even more and to define fields of fluid-mineral equilibria in the various investigated mines. The observed mineral assemblages would be in equilibrium with fluids that have Ca^{2+} activities between 10^{-4} and 10^{-1}, Mg^{2+} activities between 10^{-4} and 10^{-2} and pH values between 5 and 8.

The observed variability in textures and in the sequence of Ca-Mg arsenate occurrence testifies to changes in fluid composition during the supergene processes occurring prior to, during and after the mining of Co arsenide-bearing deposits. Changes in pH, Ca and Mg ion activities are interrelated and mainly derived from the following equilibria:

$$CaCO_3 \text{ (in vein)} + H^+ = Ca^{2+} + HCO_3^- \quad \text{(Eq. 2)}$$

$$CaMg(CO_3)_2 \text{ (in vein)} + 2\ H^+ = Ca^{2+} + Mg^{2+} + 2\ HCO_3^- \quad \text{(Eq. 3)}$$

$$CaAl_2Si_2O_8 \text{ (in host granite)} + 2\ H^+ + H_2O = Al_2Si_2O_5(OH)_4 + Ca^{2+} \quad \text{(Eq. 4)}$$

Equilibrium 4 can be modified for the formation of (observed) illite instead of (not observed) kaolinite:

$$3\ CaAl_2Si_2O_8 + 2\ K^+ + 2\ H^+ + H_2O = 2\ KAl_3Si_3O_{10}(OH)_2 + 2\ Ca^{2+} \quad \text{(Eq. 5)}$$

Hence, increasing Ca and Mg ion activities typically also lead to an increase in pH. On the contrary, precipitation of calcite in association with the Ca-Mg arsenates decreases both Ca^{2+} activity and pH (inverse of Eq. 2), and precipitation of the Ca-Mg arsenates themselves typically reduces Ca and Mg ion activities at decreasing pH according to equilibria like:

$$3\ Mg^{2+} + 2\ H_2AsO_4^- + 8\ H_2O = Mg_3(AsO_4)2{*}8\ H_2O + 4\ H^+ \quad \text{(Eq. 6)}$$

hörnesite

Also precipitation of an important phase like pharmacolite results in decreasing pH due to the reaction:

$$Ca^{2+} + H_2AsO_4^- + H^+ = CaHAsO_4 + 2\ H^+ \quad \text{(Eq. 7)},$$

although it is also possible to precipitate pharmacolite as follows:

$$Ca^{2+} + HAsO_4^{2-} = CaHASO_4 \quad \text{(Eq. 8)}$$

This is a preprint, the final version is subject to change, of the American Mineralogist (MSA)
Cite as Authors (Year) Title. American Mineralogist, in press.
(DOI will not work until issue is live.) DOI: http://dx.doi.org/10.2138/am.2014.4540

In any case, dissolution of the various minerals and precipitation of various combinations of erythrite, calcite and Ca-Mg arsenates fully explain fluctuations in Ca and Mg ion concentrations and in pH, which drive a supergene fluid into various stability fields of **Fig. 7**. In turn, this means that these assemblages are able to buffer - to some extent - the fluid compositions they are in equilibrium with. Last, but not least, the precipitation of the various arsenate minerals significantly reduces the mobility of Co and As in the environment, and this happens close to the source. Thus, these assemblages are effective inhibitors (or, at least, reducers) of Co and As mobility.

A quantitative model of fluid-mineral interaction using PHREEQC

For a quantitative understanding of fluid-mineral interaction, we used the PHREEQC code with its WATEQ4f database (Parkhurst and Appelo, 1999, Ball and Nordstrom, 1991) and the water analysis 15Mi7 from the Anton mine which contains 4 µg/l Co and 15 µg/l As, i. e. natural background levels. The model was calculated in the following way **(Fig. 8):**

1. Before the first fluid-mineral reaction:
    a. The 15Mi7 water was equilibrated with atmospheric O_2 and CO_2 before and during any further reaction, because we assume that the Ca-Mg arsenates form in steady contact with (O_2- and CO_2-bearing) air; this notion is corroborated by the observation, that they typically do not occur in closed, fluid-filled fractures, but they grow on mine walls or on loose blocks on mine floors where moisture rather than free-flowing fluid is present.
    b. In microsamples, for which alkalinity could not be titrated in the field ("Mi" in the sample numbers reported in table 3), the water was forced to charge neutrality by the addition of HCO_3^-
2. Reaction with host rock
    a. The water was equilibrated with kaolinite, goethite and quartz as a proxy of the heavily altered Triberg granite.
    b. The water was now and after every further reaction step checked for saturation with the following phases: erythrite, pharmacolite (being the only Ca arsenate for which thermodynamic data are available; Rodrígues-Blanco et al., 2007), spherocobaltite, calcite, barite, kaolinite, muscovite, chlorite, quartz, goethite and hematite. If any of these phases was

This is a preprint, the final version is subject to change, of the American Mineralogist (MSA)
Cite as Authors (Year) Title. American Mineralogist, in press.
(DOI will not work until issue is live.) DOI: http://dx.doi.org/10.2138/am.2014.4540

supersaturated, it was precipitated. All phases were treated as pure end members.

3. Reaction with vein minerals
   A. Reaction with skutterudite first, and subsequently with calcite in various water/mineral proportions; the skutterudite/calcite ratio was kept constant at 1:3
      a. Skutterudite 0.8 mol, calcite 2.4 mol: low water/mineral ratio
      b. Skutterudite 0.01 mol, calcite 0.03 mol: intermediate water/mineral ratio
      c. Skutterudite 0.001 mol, calcite 0.003 mol: high water/mineral ratio
   B. Reaction with calcite first, and subsequently with skutterudite in the amounts 0.01 mol calcite and 0.00003 mol skutterudite
      a. Saturation was checked with respect to calcite and spherocobaltite
      b. Saturation was checked with respect to a calcite-spherocobaltite solid solution ("cobaltocalcite").

Arsenate stabilities (Models 3Aa to 3Ac)

The results of models 3Aa to 3Ac are visualized in **Fig. 9**. After an initial drastic pH drop to pH values of 2.5 to 3.5 due to the skutterudite dissolution reaction, precipitation of pharmacolite and/or erythrite and (always finally) calcite leads to an increase in pH to about 8 and a decrease of Co to almost zero, i. e. background level. Arsenic, in contrast, only evolves back to its background value in model 3Aa, while in the other models it remains at values much higher than the starting concentration. This is probably a consequence of the missing Ca and Mg ions to precipitate more arsenates. Decreasing the skutterudite/calcite ratio would obviously change this. Equally interesting is that the succession of erythrite and pharmacolite changes: only at very low water/mineral ratios, pharmacolite is the first to precipitate, while - in accordance with our observations in nature - erythrite is the one to crystallize first under intermediate or high water/mineral ratios.

In terms of Ca/Co and carbonate/arsenate activity ratios, the reaction sequence shows substantial variations, as shown on **Fig. 10**. This shows that the concentrations of the toxic elements cobalt and arsenic drastically change within short time spans and short reaction paths, when cobalt arsenides react with oxidizing groundwaters. It also shows, however, how the arsenates can return the water to low levels of toxic elements

This is a preprint, the final version is subject to change, of the American Mineralogist (MSA)
Cite as Authors (Year) Title. American Mineralogist, in press.
(DOI will not work until issue is live.) DOI: http://dx.doi.org/10.2138/am.2014.4540

when precipitating. For cobalt this is shown in the predominance diagrams of **Fig. 11**. Depending on the water/mineral ratio, the paths differ in their details, but invariably return cobalt concentrations to background levels.

Carbonate stabilities (Models 3Ba and 3Bb)

Models 3Ba and 3Bb were specifically designed to investigate the stability of spherocobaltite versus Co-bearing calcite ("cobaltocalcite") in As-bearing systems. For this purpose, both the stabilities of pure spherocobaltite and calcite end members and of a solid solution between calcite and spherocobaltite were modeled. Guggenheim parameters used in the asymmetric calcite-spherocobaltite mixing model are from Katsikopoulos et al. (2008) and were inserted to PHREEQC. Despite the inherent uncertainties in the thermodynamic data (see Katsikopoulos et al., 2008; Egorov et al., 1976; Gamsjäger & Reiter, 1979), we believe that it is possible to derive interesting insights from these models.

The major difference to the models before lies in the fact that the fluid reacts with calcite prior to reacting with skutterudite, and that the amount of skutterudite oxidized is vanishingly small (skutterudite/calcite ratio of 0.003) compared to the models above. Testing the setup of models 3Ba and 3Bb, this was the only way to stabilize spherocobaltite in contrast to erythrite at all. As **Figs. 12-14** show, both end member spherocobaltite and a Co-dominated carbonate solid solution have only very small stability fields **(Fig. 14)** and are after the very first increments of skutterudite oxidation (which causes them to precipitate, see **Fig. 13**) immediately destabilized with respect to erythrite. In this model, pH increases due to calcite dissolution in the beginning and stays high (above 8) during the whole fluid-mineral interaction process. The abundant occurrence of calcite sinters colored pink by the incorporation of small amounts (below the microprobe's detection limit on the EDX system) of Co in the neighborhood of weathering skutterudite and other cobalt arsenides and the rarity of real spherocobaltite fit very well with our calculations: as shown by Katsikopoulos et al. (2008) and Kornicker et al. (1985), Co is preferentially incorporated into calcite when in equilibrium with a Co-bearing water. Hence, a carbonate-rich Co-bearing fluid with background levels of Co and As in the ppb level is below the saturation with erythrite and will precipitate Co-bearing calcite. This precipitation reaction will further decrease the Co concentration in the fluid significantly. Reaction of this oxidizing fluid with a Co arsenide phase like skutterudite will stabilize spherocobaltite over a very small reaction

This is a preprint, the final version is subject to change, of the American Mineralogist (MSA)
Cite as Authors (Year) Title. American Mineralogist, in press.
(DOI will not work until issue is live.) DOI: http://dx.doi.org/10.2138/am.2014.4540

interval, before erythrite precipitation again buffers Co to very low levels. This behavior shows that both carbonate and erythrite precipitation are able to scavenge Co from natural solutions almost completely. Furthermore, it explains the rarity of the Co end member spherocobaltite in nature. The reaction

$$\text{safflorite} + 2\ H_2O + 3\ O_2 = Co^{2+} + 2\ H_2AsO_4^-$$

releases two arsenate ions for one cobalt ion and hence, decreases the Co/As ratio, immediately driving the fluid composition invariably towards erythrite saturation. Subsequent precipitation of erythrite,

$$3\ Co^{2+} + 2\ H_2AsO_4^- + 8\ H_2O = \text{erythrite} + 4\ H^+,$$

further decreases the Co/As ratio so that as soon as erythrite stability is reached, it becomes impossible to reach spherocobaltite saturation, as not only the Co concentration, but also the Co/As ratio of upper crustal fluids decrease rapidly. As a consequence, spherocobaltite can only be stabilized in As-free systems where e. g. carrollite is a major primary Co ore. Hence, it is not surprising that the carrollite-bearing deposits of Katanga in the Democratic Republic of Kongo are the only major source of macroscopic spherocobaltite specimens worldwide.

Implications

The observations of naturally occurring Co-Ca-Mg arsenates combined with calculated fluid-rock interaction models presented in this contribution not only explain the common occurrence of erythrite and some minerals like pharmacolite or picropharmacolite in and around Co-bearing ore deposits, but they also provide a semiquantitative to quantitative framework for Co and As immobilization at and around such locations. The stability of erythrite buffers Co at very low values, the stability of Ca-Mg arsenates further lowers As concentrations, the details depending on the little investigated, but here described highly variable phase assemblages. The rarity of spherocobaltite (Co carbonate) and the ubiquity of erythrite (Co arsenate) is a consequence of the low solubility product of erythrite and the common association of Co together with As in primary ores.

Acknowledgements

We are grateful to Martin Herrmann, Schapbach, for providing admission to the mines, to Susanne Göb and Sebastian Staude for their help during sampling of the mine waters

and to Christoph Berthold, Nadja Huber, Melanie Keuper, Thomas Wenzel, Gabriele Stoschek, Bernd Steinhilber, Zsolt-Attila Berner and Kai Hettmann, Tübingen, for their help with sample analysis and model setup.

References

Álvarez-Valero, A. M., Péréz-López, R., Matos, J., Capitán, M. A., Nieto, J. M., Sáez, R. and Delgado, J. (2008) Carabello, M. Potential environmental impact at Sao Domingos mining district (Iberian Pyrite Belt, SW Iberian Peninsula): evidence from a chemical and mineralogical characterization. Environmental Geology, 55, 1797-1809.

Ball, J. W. and Nordstrom, D. K. (1991) User's manual for WATEQ4F, with revised thermodynamic data base and test cases for calculating speciation of major, trace, and redox elements in natural waters. United States Geological Survey Open-file report, 91-183.

Bari, H. (1983) Markirch/Elsass: Die Mineralien des berühmten Bergbaureviers. Lapis, 6, 9-37.

Brockamp, O., Clauer, N. and Zuther, M. (1998) Authigenic sericite record of a fossil geothermal system: the Offenburgh trough, central Black Forest, Germany. International Journal of Earth Sciences, 92, 843-851.

Brown G. and Calas, G. (2012) Mineral-water interfaces as driving forces for metal concentration: the example of cobalt trapping by Mn-oxides. Geochemical Perspectives, 1, 667-669.

Bucher, K. and Stober, I. (2010) Fluids in the upper continental crust. Geofluids, 10, 241-253.

Dill, H. (2010) The "chessboard" classification scheme of mineral deposits: Mineralogy and geology from aluminum to zirconium. Earth Science Reviews, 100, 1-420.

Dold, B. and Fontboté, L. (2001) Element cycling and secondary mineralogy in porphyry copper tailings as a function of climate, primary mineralogy, and mineral processing. Journal of Geochemical Exploration, 74, 3-55.

Dold, B., Wade, C. and Fontboté, L. (2009) Water management for acid mine drainage control at the polymetallic Zn-Pb-(Ag-Bi-Cu) deposit Cerro de Pasco, Peru. Journal of Geochemical Exploration, 100, 133-141.

Egorov, V. M., Ikornikova, N. Y. and Lobachev, A. N. (1976) Preparation and study of the sphaerocobaltite monocrystal solubility under hydrothermal conditions. Journal of Crystal Growth, 36, 138-146.

Fay, I. and Barton, M.D. (2012) Alteration and ore distribution in the Proterozoic Mines Series, Tenke-Fungurume Cu–Co district, Democratic Republic of Congo. Mineralium Deposita, 47, 501-519.

Gamsjäger, H. and Reiterer, F. (1979) Investigation of equilibria involving carbon dioxide, carbonates and water. Environment International, 2, 419-424.

Gervilla, F., Fanlo, I., Colás, V., and Subías, I. (2012) Mineral compositions and phase relations of Ni–Co–Fe arsenide ores from the Aghbar mine, Bou Azzer, Morocco. Canadian Mineralogist, 50, 447-470.

Göb, S., Loges, A., Nolde, N., Bau, M., Jacob, D. E. and Markl, G. (2013) Major and trace element composition (icluding REE) of mineral, thermal, mine and surface waters in SW Germany and implications for water-rock interaction. Applied Geochemistry, 33, 127-152.

Hlousek, J. and Tvrdy, J. (2002) Interessante Sekundärmineralien aus Jáchymov. Lapis, 27, 7-8, 44-66.

Juillot, F., Ildefonse, P., Morin, G., Calas, G., Kersabiec, A. and Benedetti, M. (1999) Remobilization of arsenic from buried wastes at an industrial site: mineralogical and geochemical control. Applied Geochemistry, 14, 1031-1048.

Karsten, D.L.G. (1800) Mineralogische Tabellen, Berlin, 245 p.

Katsikopoulos, D., Fernández-González, Á., Prieto, A. C. and Prieto, M. (2008) Co-crystallization of Co(II) with calcite: Implications for the mobility of cobalt in aqueous environments. Chemical Geology, 254, 87-100.

Kornicker, W. A., Morse, J. W. and Damasceno, R. N. (1985) The chemistry of Co^{2+} interaction with calcite and aragonite surfaces. Chemical Geology, 53, 229-236.

Lefebure D. V. (1996) Five-element veins Ag-Ni–Co–As +/− (Bi, U). In: Lefebure, D.V. and Höy, T. (eds) Selected British Columbia mineral deposit profiles, vol. 2—metallic deposits. British Columbia Ministry of Employment and Investment Open File, 13, 89–92.

Markl, G. (2005) Bergbau und Mineralienhandel im fürstenbergischen Kinzigtal, Markstein Verlag, Filderstadt, Germany, 448 p.

Markl, G. and Slotta, C. (2011) Die Uranmineralien des Lagerstättenreviers von Wittichen im mittleren Schwarzwald. Lapis, 36, 25-37.

Martins, U. and Pfefferkorn, H. (1988) Genetic interpretation of a lower Triassic paleosol complex based on soil micromorphology. Paleogeography Paleoclimatology Paleoecology, 64, 1-14.

Massanek, A. and Michalski, S. (2005) Die Mineralien des Schneeberger Reviers. Lapis, 30, 7-8, 41-82.

Parkhurst, D. L. and Appelo, C. A. J. (1999) User's guide to PHREEQC (Version 2) – A computer program for speciation, batch-reaction, one-dimensional transport, and inverse geochemical calculations, United States Geological Survey Water-Resources Investigations Report, 99-4259.

Pierrot, R. (1964) Contribution à la minéralogie des arséniates calciques et calcomagnésiens naturels. Bulletin de la Societé Francaise de Minéralogie et Cristallographie, 87, 169-211.

Rodrígues-Blanco, J. D., Jiménez, A. and Proeto, A. (2007) Oriented overgrowth of pharmacolite ($CaHAsO_4*2H_2O$) on gypsum ($CaSO_4*2H_2O$), Crystal Growth, 7, 2756-2763.

Schnorrer-Köhler, G. (1983) Die Minerale des Richelsdorfer Gebirges. Der Aufschluß, 34, 535-540.

Selb, K. J. (1800) Über arseniksauren Kalk von Wittichen. Allgemeines Journal für Chemie, 4, 537.

Slack, J. F., Causey, J. D., Eppinger, R. G., Gray, J. E., Johnson, C. A., Lund, K. I. and Schulz, K. J. (2010) Co-Cu-Au Deposits in Metasedimentary Rocks. A Preliminary Report. United States Geological Survey Open-File Report, 2010–1212.

Staude, S., Mordhorst, T., Nau, S., Pfaff, K., Brügmann, G., Jacob, D. E. and Markl, G. (2012a) Hydrothermal carbonates of the Schwarzwlad ore district, Southwestern Germany: Carbon source and conditions of formation using $\delta^{18}O$, $\delta^{13}C$, $^{87}Sr/^{86}Sr$, and fluid inclusions. Canadian Mineralogist, 50, 1401-1434.

Staude, S., Werner, W., Mordhorst, T., Wemmer, K., Jacob, D. E. and Markl, G. (2012b) Multi-stage Ag-Bi-Co-Ni-U and Cu-Bi vein mineralization at Wittichen, Schwarzwald, SW Germany: geological setting, ore mineralogy, and fluid evolution. Mineralium Deposita, 47, 251-276.

Tvrdy, J. and Karlovy, V. (2002) Geologie und Erzgänge des Reviers Jáchymov. 27, 7-8, 27-30.

Valente, T. M. and Gomes, C. L. (2009) Occurrence, properties and pollution potential of environmental minerals in acid mine drainage. Science of the Total Environment, 407, 1135-1152.

This is a preprint, the final version is subject to change, of the American Mineralogist (MSA)
Cite as Authors (Year) Title. American Mineralogist, in press.
(DOI will not work until issue is live.) DOI: http://dx.doi.org/10.2138/am.2014.4540

564 Vogelsang, W. M. (1865) Geognostisch-bergmännische Beschreibung des Kinzigthaler
565 Bergbaues. Beiträge zur Statistik der inneren Verwaltung des Großherzogthums
566 Baden, 21, 1-146.
567 Walenta, K. (1972) Die Sekundärmineralien der Co-Ni-Ag-Bi-U-Erzgänge im Gebiet von
568 Wittichen im mittleren Schwarzwald. Der Aufschluß, 23, 279-329.
569 Walenta, K. (1987) Wittichen. Lapis, 12, 13-55.
570 Walenta, K. (1992) Die Mineralien des Schwarzwaldes und ihre Fundstellen, Weise
571 Verlag, München, Germany, 202 p.
572 Walenta, K. and Dunn, P. (1989) Camgasit, ein neues Calcium-Magnesiumarsenatmineral
573 der Zusammensetzung $CaMg(AsO_4)(OH)*5H_2O$ von Wittichen im mittleren
574 Schwarzwald. Der Aufschluß, 40, 369-372.
575
576
577 **Figure captions**
578
579 **Figure 1:** Geological map of the Wittichen area in the Central Schwarzwald, SW
580 Germany together with sample localitites.
581
582 **Figure 2:** Examples of mineral samples used in this study. (A) Pharmacolite and
583 picropharmacolite deposited on a massive skutterudite vein in reddish granitic host
584 rock; width of photograph (WOP) is about 8 cm. (B) Picropharmacolite and little
585 erythrite in calcite; WOP about 10 cm. (C) Pharmacolite aggregate on a barren granite
586 fracture. WOP about 5 cm. (D) Picropharmacolite on pharmacolite on barren granite,
587 WOP about 10 cm. (E) Picropharmacolite on wendwilsonite on pink erythrite; WOP is
588 about 6 mm. (F) Colorless ferrarisite with white pharmacolite on erythrite; WOP is
589 about 6 mm. (G) Colorless pharmacolite on white crust of hörnesite, overgrowing pink
590 erythrite; WOP is about 1 cm. (H) Rosette of white wendwilsonite with needles of
591 pharmacolite on pale pinkish erythrite-hörnesite solid solution. WOP is about 6 mm.
592
593 **Figure 3:** Examples of sampling sites for water samples used in this study. (A) White
594 calcite sinter in the mine Michael im Rohrbächle near Schiltach (08Mi2), WOP is around
595 30 cm. (B) Purple calcite sinter in the mine Frisch Glück, Wittichen (12Mi5), WOP is
596 around 25 cm. (C) Purple calcite sinter in the mine Frisch Glück, Wittichen (12Mi3),
597 WOP is around 10 cm. (D) Brown iron oxide-bearing sinter in the mine Anton,

598 Heubachtal (15Mi5), WOP is around 15 cm. (E) Calcite sinter in the mine Frisch Glück,
599 Wittichen (12Mi4), WOP is around 10 cm. (F) Erythrite (purple) associated with a
600 yellowish uranyl-arsenate in the mine Anton, Heubachtal (15Mi2), WOP is around 5 cm.
601
602 **Figure 4:** Overview of the studied water samples. (A) pH values versus conductivities.
603 (B) Major cations and anions illustrated in a Piper diagram.
604
605 **Figure 5:** Ca, Mg, Co, Ni and As concentration data of the studied water samples.
606
607 **Figure 6:** IMA-approved mineral species in the system Ca-Mg-As. Note that
608 wendwilsonite and roselite contain significant amounts of Co compared to talmessite.
609
610 **Figure 7:** Activity-activity diagram in the Ca-Mg-As system taking into account the
611 observed mineral assemblages in mines of the Wittichen area, Germany. Note that X-
612 and Y-axis were quantified based on measured pH values and Ca and Mg concentrations
613 of the water samples used in this study. The large green, yellow and pink fields overlap
614 each other, i.e., they are not meant to represent a zonation.
615
616 **Figure 8:** Flow chart illustrating the different approaches to model fluid-mineral
617 interaction using the PHREEQC code and the water analysis 15Mi7 from the Anton mine
618 which contains 4 µg/l Co and 15 µg/l As, i. e. natural background levels.
619
620 **Figure 9:** Results of models 3Aa, 3Ab and 3Ac (representing low, intermediate and high
621 fluid/mineral ratios) showing the evolution of pH, the timing and amount of mineral
622 precipitation (erythrite, pharmacolite and calcite) and the changes in As, Co and Ca
623 concentrations in the solution during reaction with skutterudite and calcite. The units
624 are moles or mmoles of the respective minerals which react with 1 l of water.
625
626 **Figure 10:** Evolution of Ca/Co and carbonate/arsenate activity ratios in mine waters
627 based on models 3Aa, 3Ab and 3Ac. The black dot represents the composition of water
628 sample 15Mi7 after equilibration with quartz, goethite and kaolinite at 10 °C and
629 atmospheric O_2 and CO_2. White squares indicate the start of reaction with skutterudite,
630 circles the subsequent reaction with calcite. The lines illustrate the changes in activity
631 ratios during reaction with skutterudite and calcite, respectively. These lines are

This is a preprint, the final version is subject to change, of the American Mineralogist (MSA)
Cite as Authors (Year) Title. American Mineralogist, in press.
(DOI will not work until issue is live.) DOI: http://dx.doi.org/10.2138/am.2014.4540

stippled if no intermediate steps were calculated, i. e., if the change in composition occurred very fast between to calculation steps, while continuous lines indicate that they occurred more smoothly.

Figure 11: Activity diagrams for Co and Ca with predominance fields of erythrite and picropharmacolite for different pH values. (A) The qualitative effects of skutterudite and calcite dissolution, respectively, are indicated by grey arrows. (B) – (D) Similar diagrams showing the results of the model 3Aa to 3Ac. White and purple stars symbolize precipitation of picropharmacolite and erythrite, respectively.

Figure 12: Results for carbonate stabilities based on models 3Ba (calcite and spherocobaltite) and 3Bb ("cobaltocalcite") showing the evolution of pH, the timing and amount of mineral precipitation (calcite, spherocobaltite, "cobaltocalcite" and erythrite), changes in the composition of "cobaltocalcite" and the changes in As, Co, Ca and C concentrations in the solution during reaction with calcite and then skutterudite. Units are, as in Fig. 9, mmoles and µmoles per 1 l water.

Figure 13: Evolution of Ca/Co and carbonate/arsenate activity ratios in mine waters based on models 3Ba and 3Bb. The black dot represents the composition of water sample 15Mi7 after equilibration with quartz, goethite and kaolinite at 10 °C and atmospheric O_2 and CO_2. White circles indicate the start of reaction with calcite, squares the subsequent reaction with skutterudite. As in Fig. 10, these lines are stippled if no intermediate steps were calculated, i. e., if the change in composition occurred very fast between to calculation steps, while continuous lines indicate that they occurred more smoothly.

Figure 14: Activity diagram for Co and Ca (A) with predominance fields of spherocobaltite (purple) and calcite for different pH values. The stability field of erythrite is superimposed; increasing the arsenic concentration results in the stabilization of erythrite relative to spherocobaltite. The black arrow illustrates the evolution of water in equilibrium with calcite during dissolution of skutterudite, crossing the stability field of spherocobaltite, which is only stable at low arsenic concentrations. (B) Mixing lines of "cobaltocalcite" in equilibrium with water sample 15Mi07 for different pH values. The X_{Sph} values of 0.95 and 0.16 are indicated as dashed

666 lines, based on the proposed miscibility gap in the system calcite-spherocobaltite after
667 Katsikopoulos et al. (2008).

Figure 1

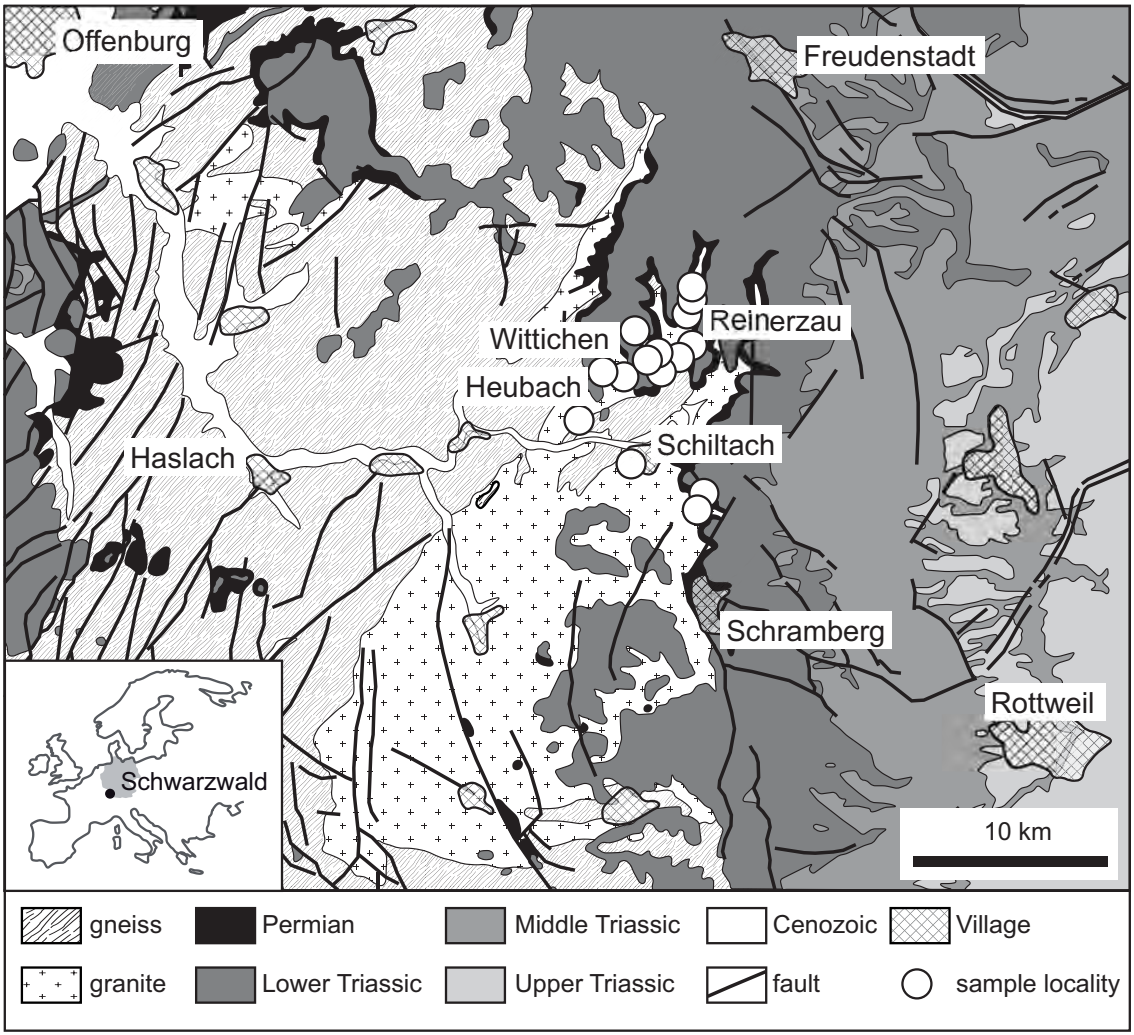
Offenburg
Freudenstadt
Reinerzau
Wittichen
Heubach
Schiltach
Haslach
Schramberg
Rottweil
Schwarzwald
10 km
gneiss
granite
Permian
Lower Triassic
Middle Triassic
Upper Triassic
Cenozoic
fault
Village
sample locality

Figure 2

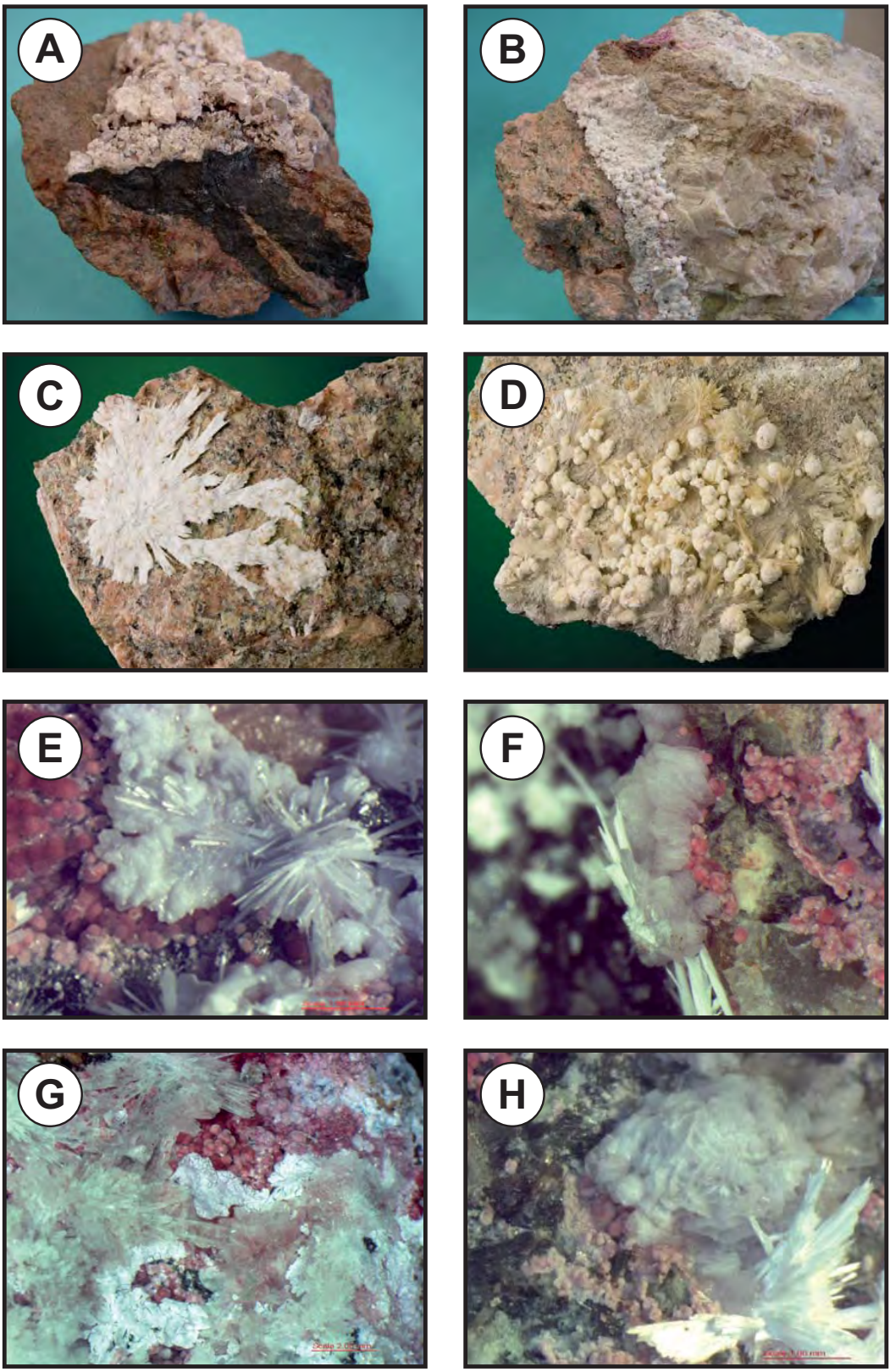

Figure 3

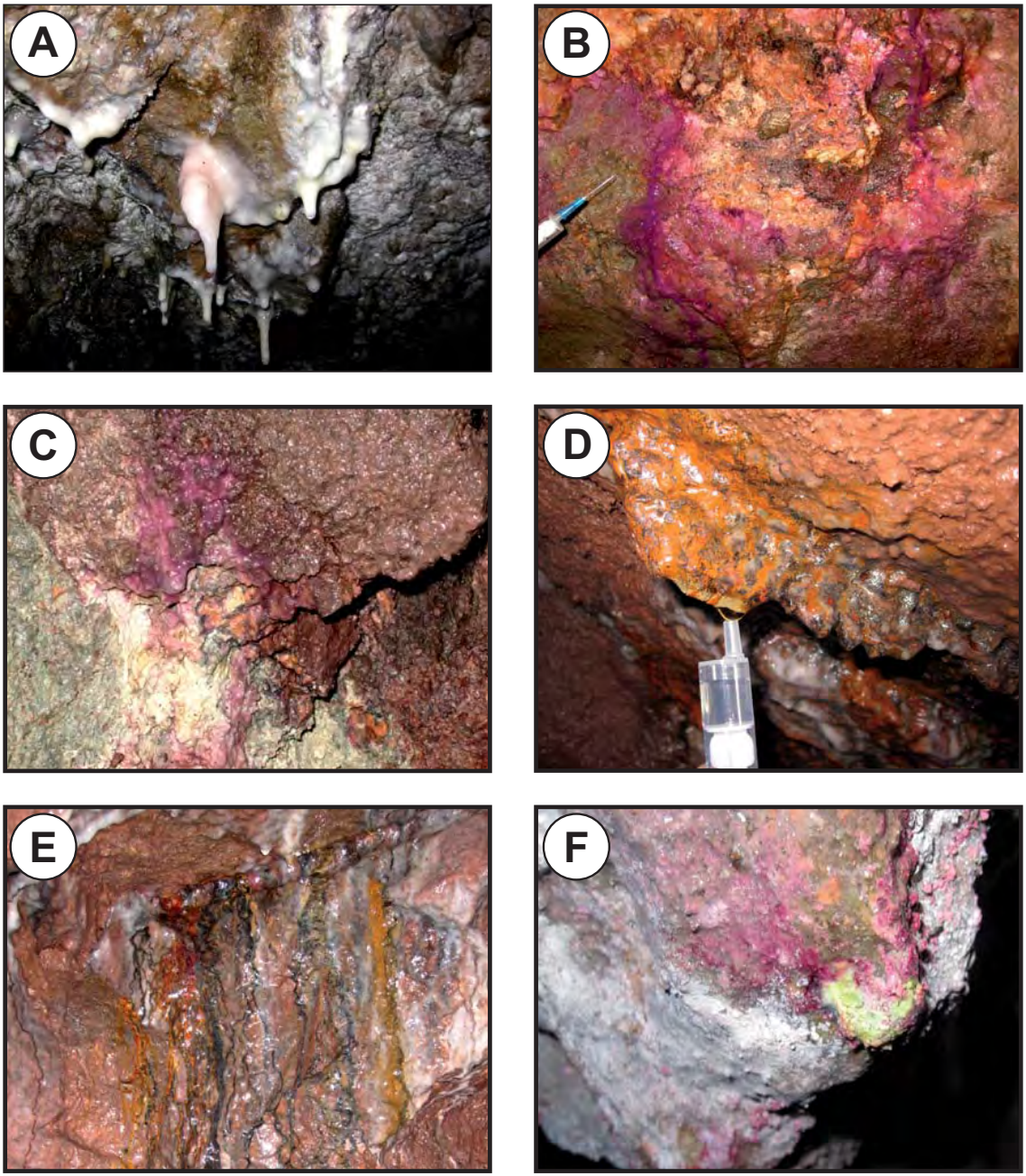

Figure 4

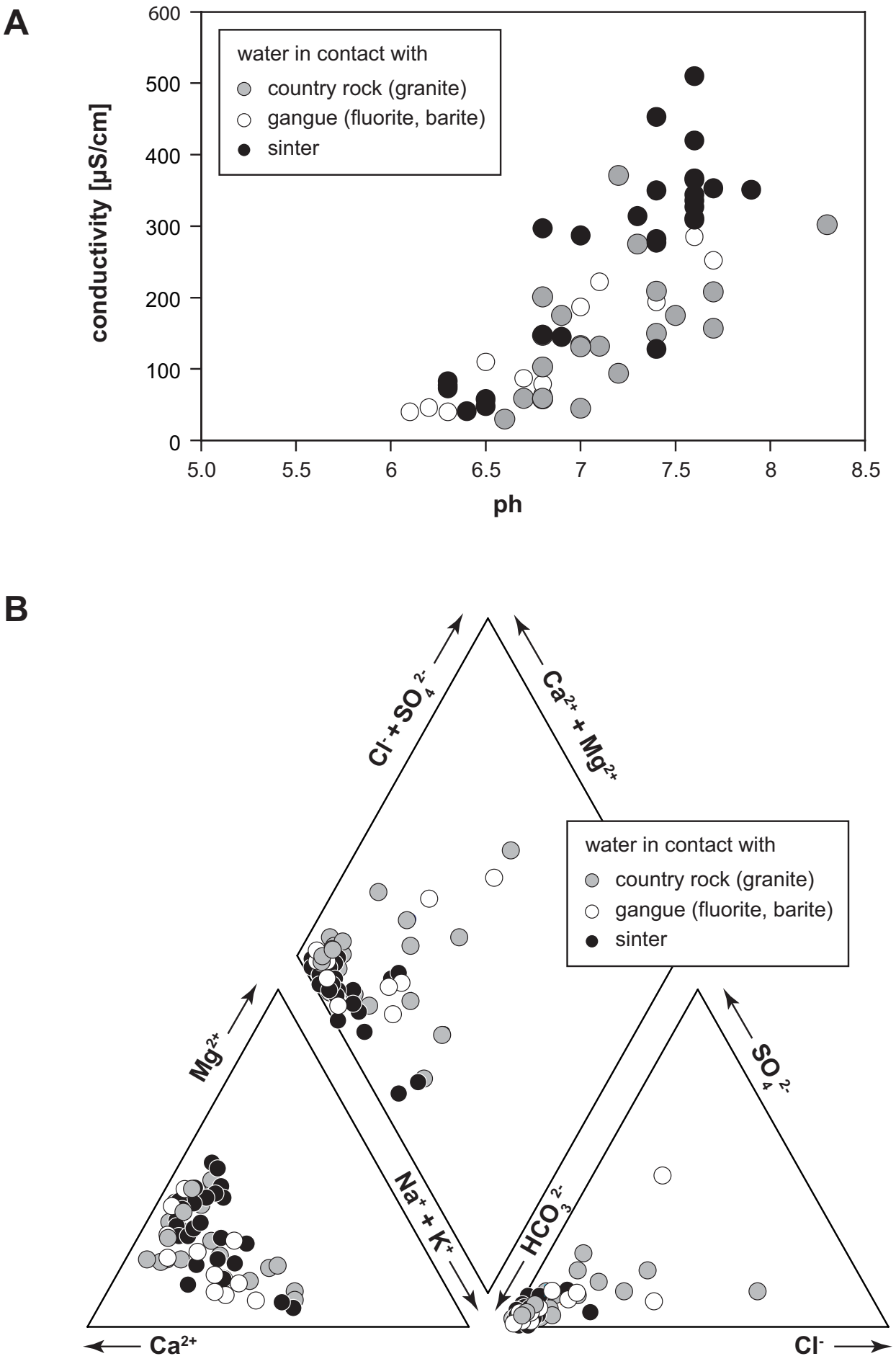
A
conductivity [µS/cm]
ph
water in contact with
country rock (granite)
gangue (fluorite, barite)
sinter
B
Cl⁻ + SO4 2-
Ca2+ + Mg2+
Mg2+
Na+ + K+
HCO3 2-
SO4 2-
Ca2+
Cl⁻
water in contact with
country rock (granite)
gangue (fluorite, barite)
sinter

Figure 5

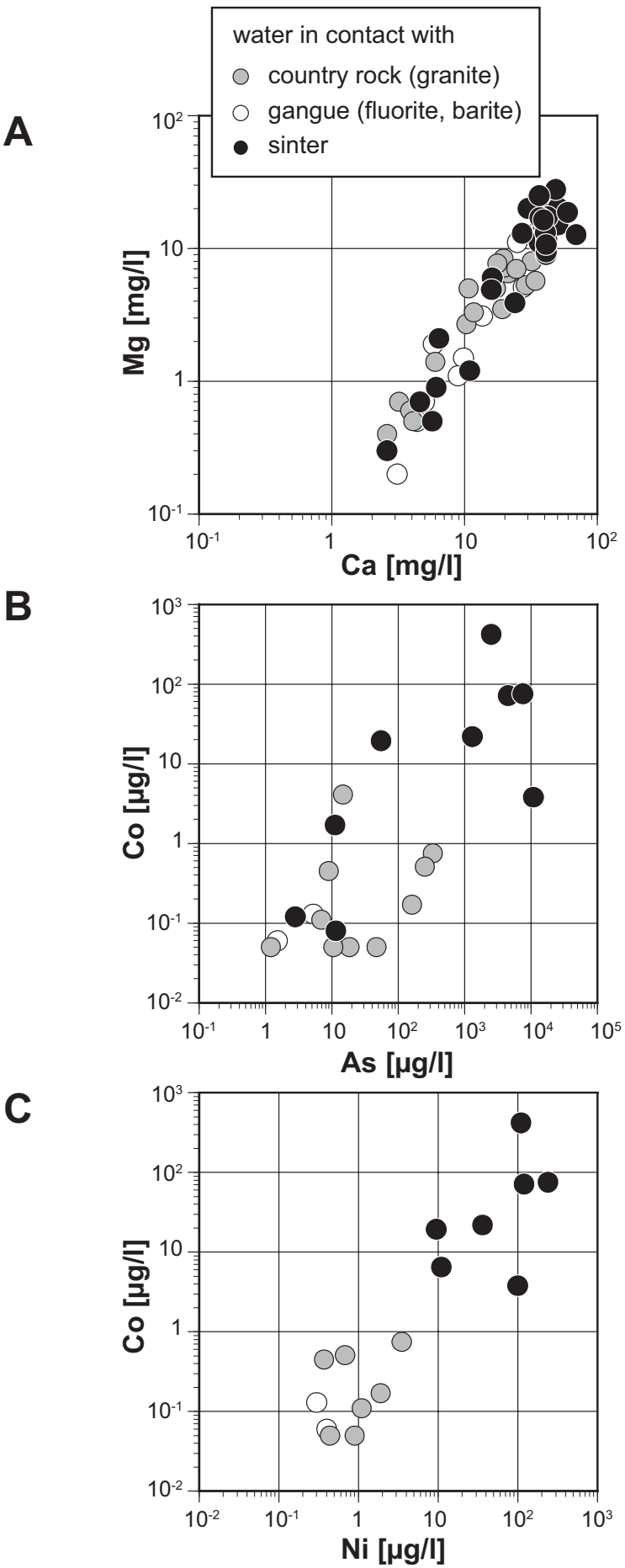
A
water in contact with
country rock (granite)
gangue (fluorite, barite)
sinter
Mg [mg/l]
Ca [mg/l]
B
Co [µg/l]
As [µg/l]
C
Co [µg/l]
Ni [µg/l]

Figure 6

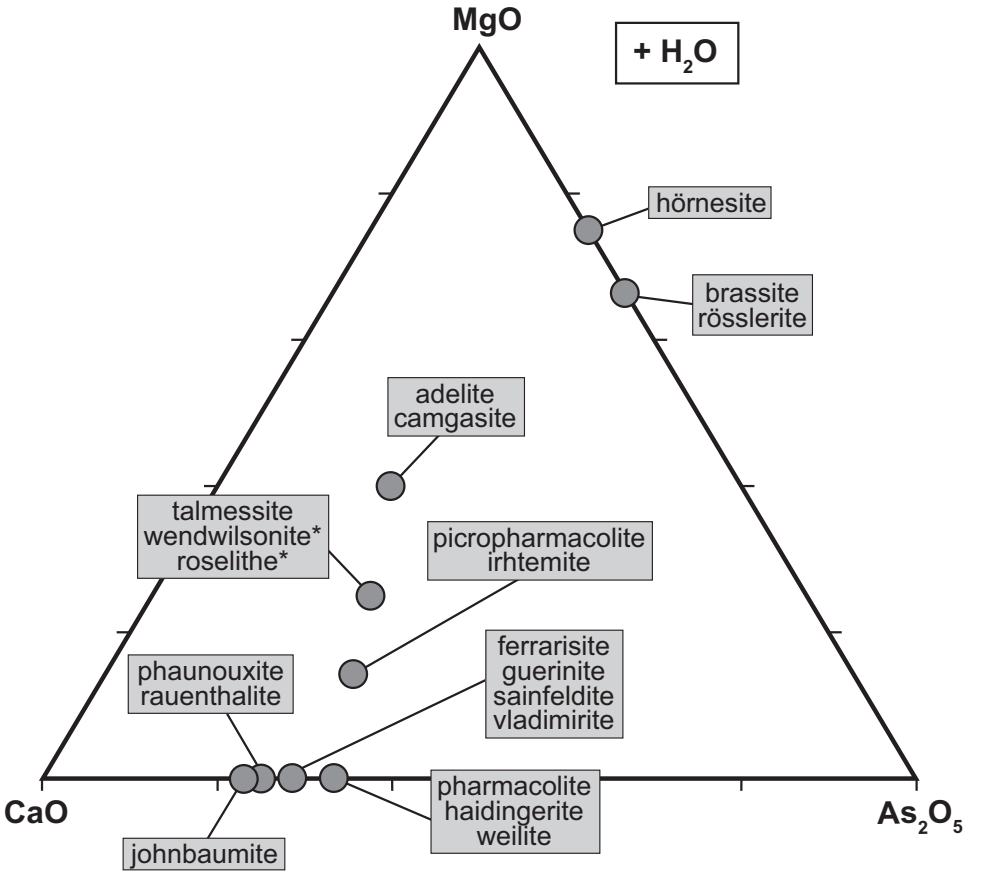
MgO
+ H2O
hörnesite
brassite
rösslerite
adelite
camgasite
talmessite
wendwilsonite*
roselithe*
picropharmacolite
irhtemite
ferrarisite
guerinite
sainfeldite
vladimirite
phaunouxite
rauenthalite
pharmacolite
haidingerite
weilite
CaO
As2O5
johnbaumite

Figure 7

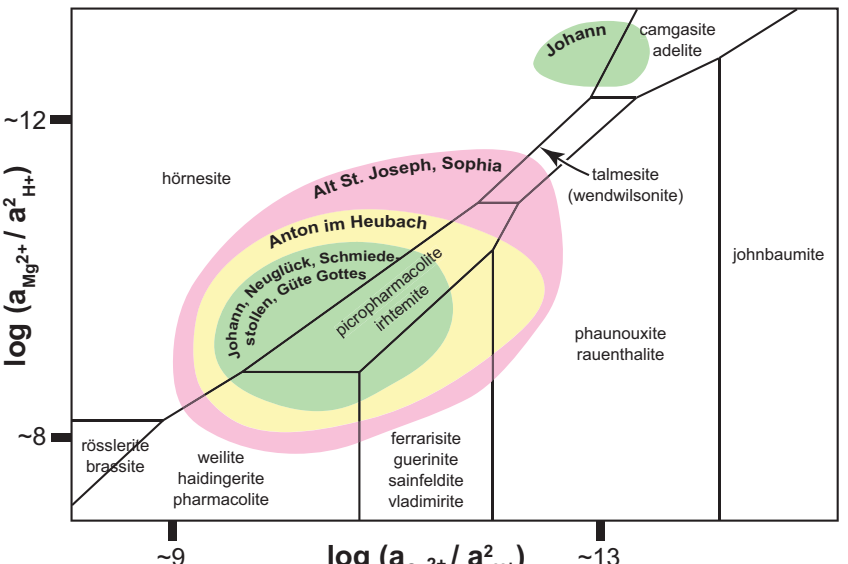
Johann
camgasite
adelite
~12
hörnesite
Alt St. Joseph, Sophia
talmesite
(wendwilsonite)
Anton im Heubach
Johann, Neuglück, Schmiede-
stollen, Güte Gottes
picropharmacolite
irhtemite
johnbaumite
phaunouxite
rauenthalite
log (a Mg2+ / a2 H+)
~8
rösslerite
brassite
weilite
haidingerite
pharmacolite
ferrarisite
guerinite
sainfeldite
vladimirite
~9
log (a Ca2+ / a2 H+)
~13

Figure 8

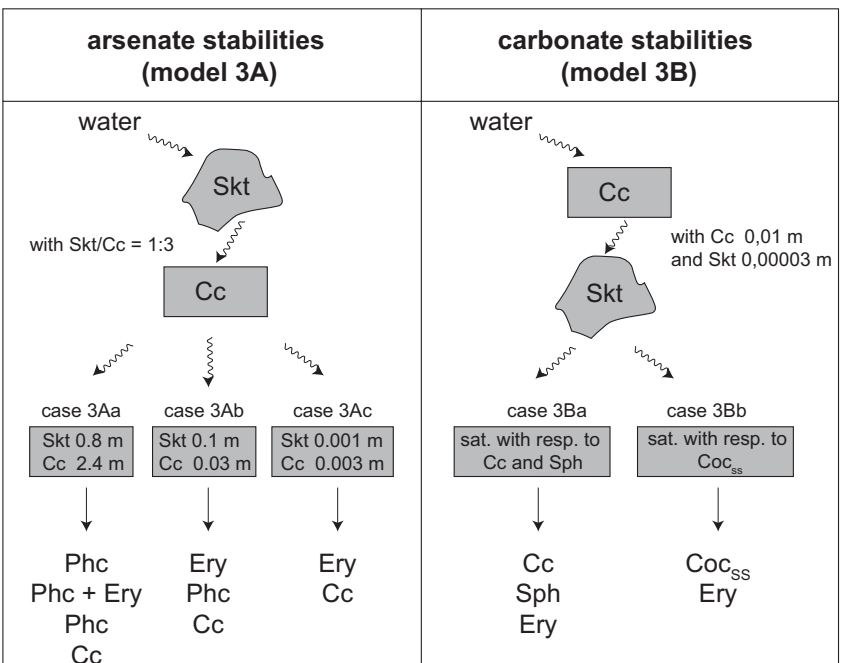

Skt = skutterudite; Cc = calcite; Phc = pharmacolite; Ery = erythrite; Sph = spherocobaltite; Coc = cobaltocalcite; $_{ss}$ = solid solution

Figure 9

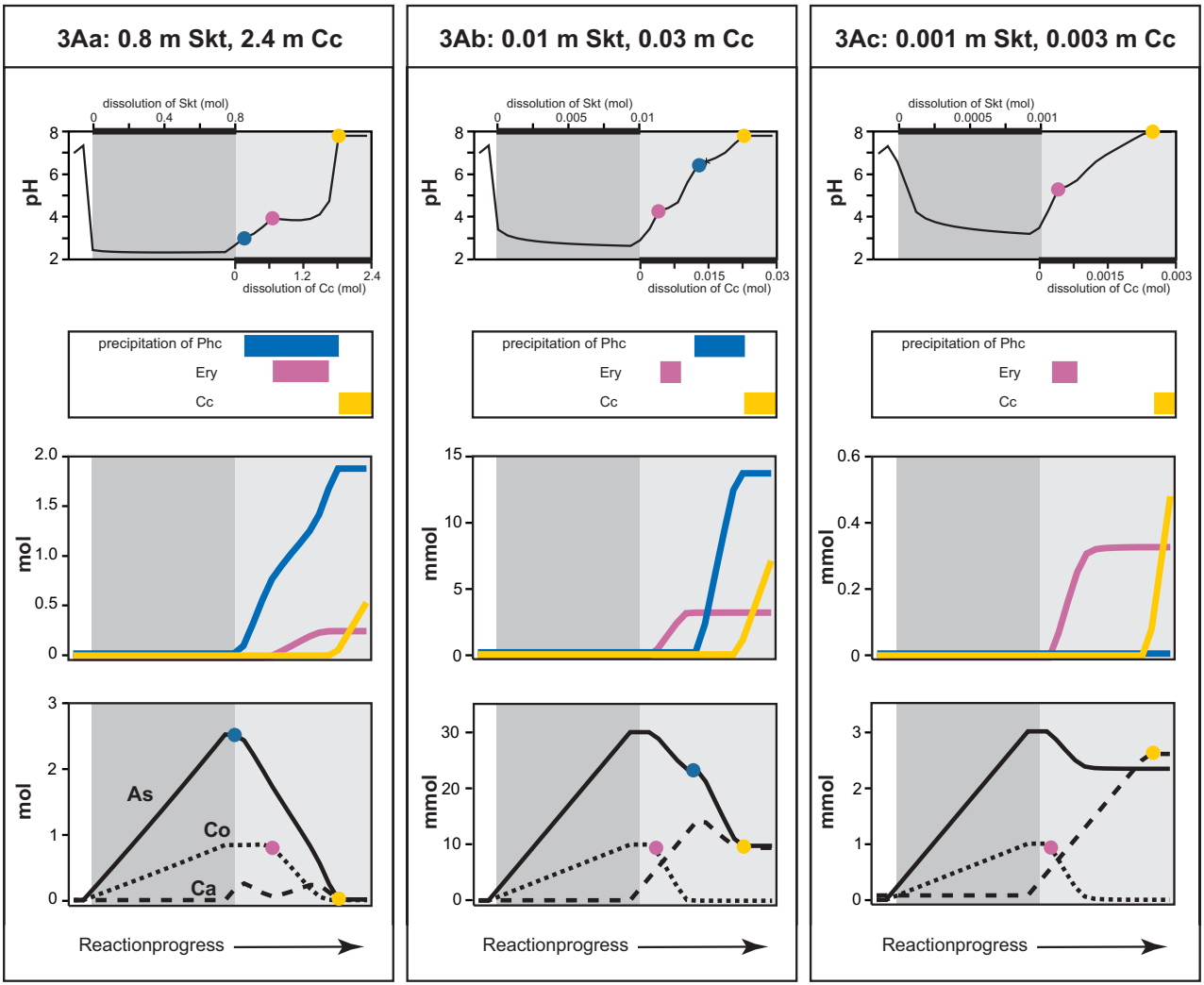
3Aa: 0.8 m Skt, 2.4 m Cc
3Ab: 0.01 m Skt, 0.03 m Cc
3Ac: 0.001 m Skt, 0.003 m Cc
dissolution of Skt (mol)
pH
dissolution of Cc (mol)
precipitation of Phc
Ery
Cc
mol
mmol
As
Co
Ca
Reactionprogress

Figure 10

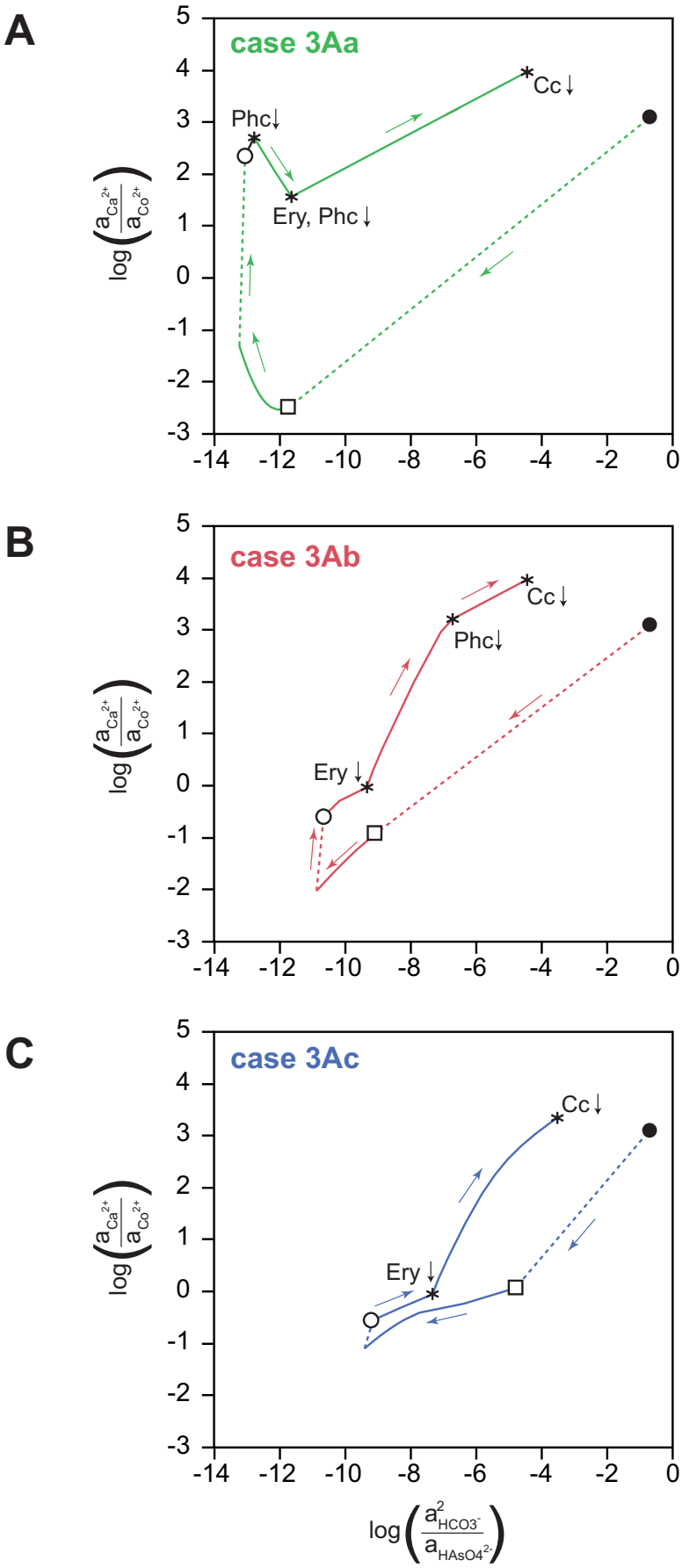
A
case 3Aa
Cc↓
Phc↓
Ery, Phc↓
B
case 3Ab
Cc↓
Phc↓
Ery↓
C
case 3Ac
Cc↓
Ery↓
log(a_Ca2+ / a_Co2+)
log(a²_HCO3- / a_HAsO4 2-)

Figure 11

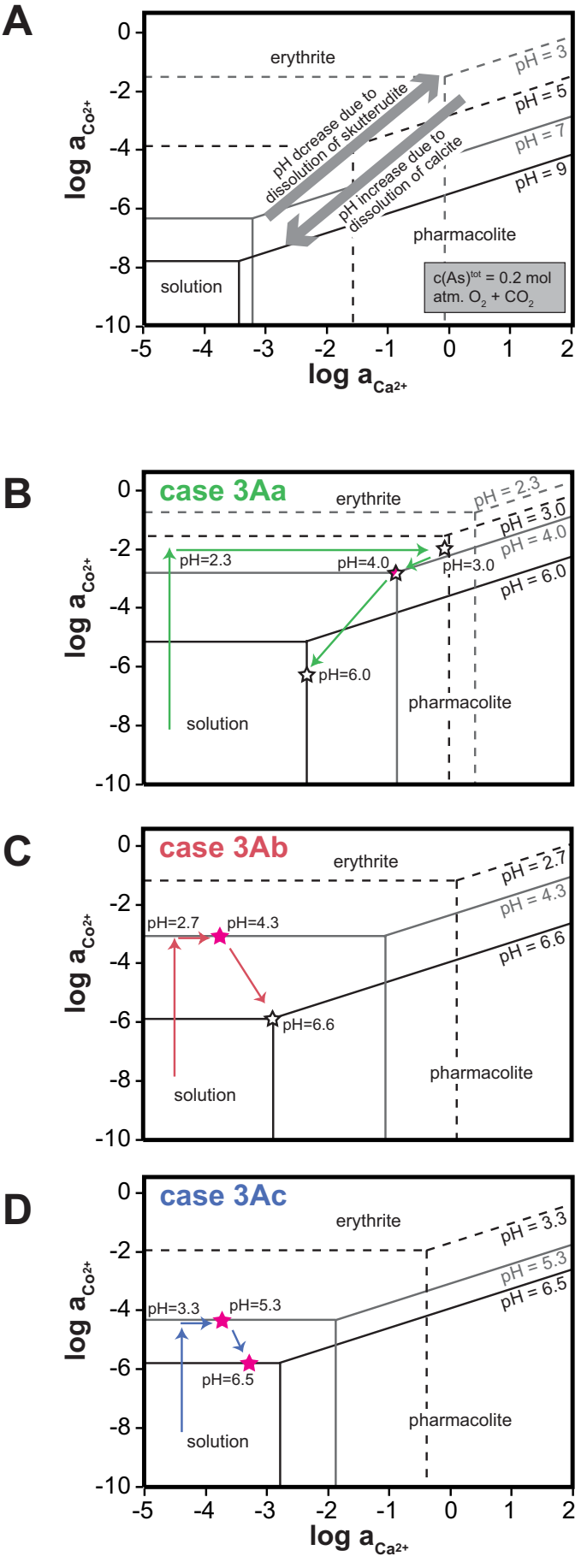
A
erythrite
pH = 3
pH = 5
pH = 7
pH = 9
pH decrease due to dissolution of skutterudite
pH increase due to dissolution of calcite
pharmacolite
solution
c(As)tot = 0.2 mol
atm. O2 + CO2
log aCo2+
log aCa2+
B
case 3Aa
erythrite
pH = 2.3
pH = 3.0
pH = 4.0
pH = 6.0
pH=2.3
pH=4.0
pH=3.0
pH=6.0
pharmacolite
solution
C
case 3Ab
erythrite
pH = 2.7
pH = 4.3
pH = 6.6
pH=2.7
pH=4.3
pH=6.6
pharmacolite
solution
D
case 3Ac
erythrite
pH = 3.3
pH = 5.3
pH = 6.5
pH=3.3
pH=5.3
pH=6.5
pharmacolite
solution

Figure 12

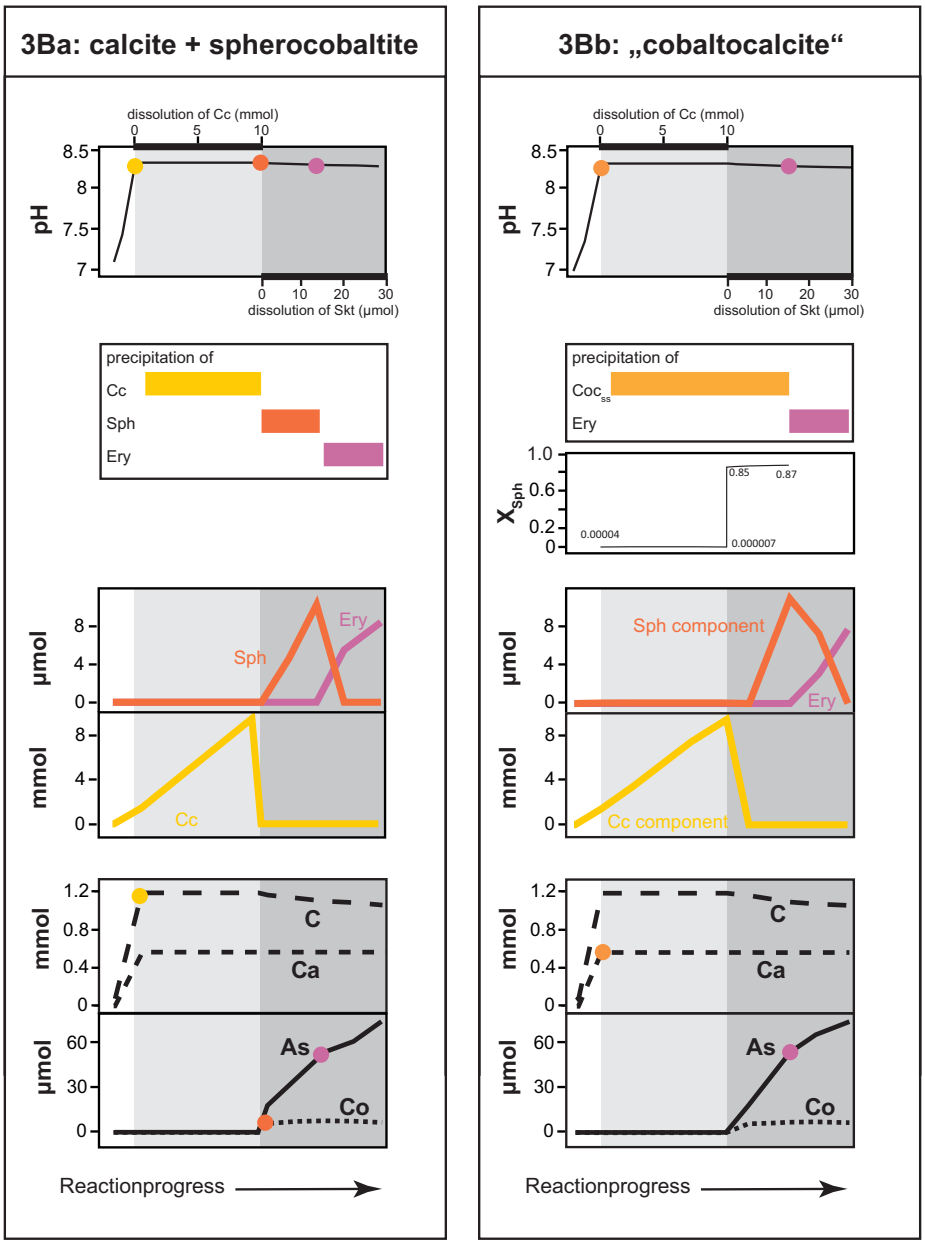
3Ba: calcite + spherocobaltite
3Bb: „cobaltocalcite“
dissolution of Cc (mmol)
pH
dissolution of Skt (µmol)
precipitation of
Cc
Sph
Ery
Coc$_{ss}$
X_{Sph}
0.85
0.87
0.00004
0.000007
µmol
mmol
Sph component
Cc component
C
Ca
As
Co
Reactionprogress

Figure 13

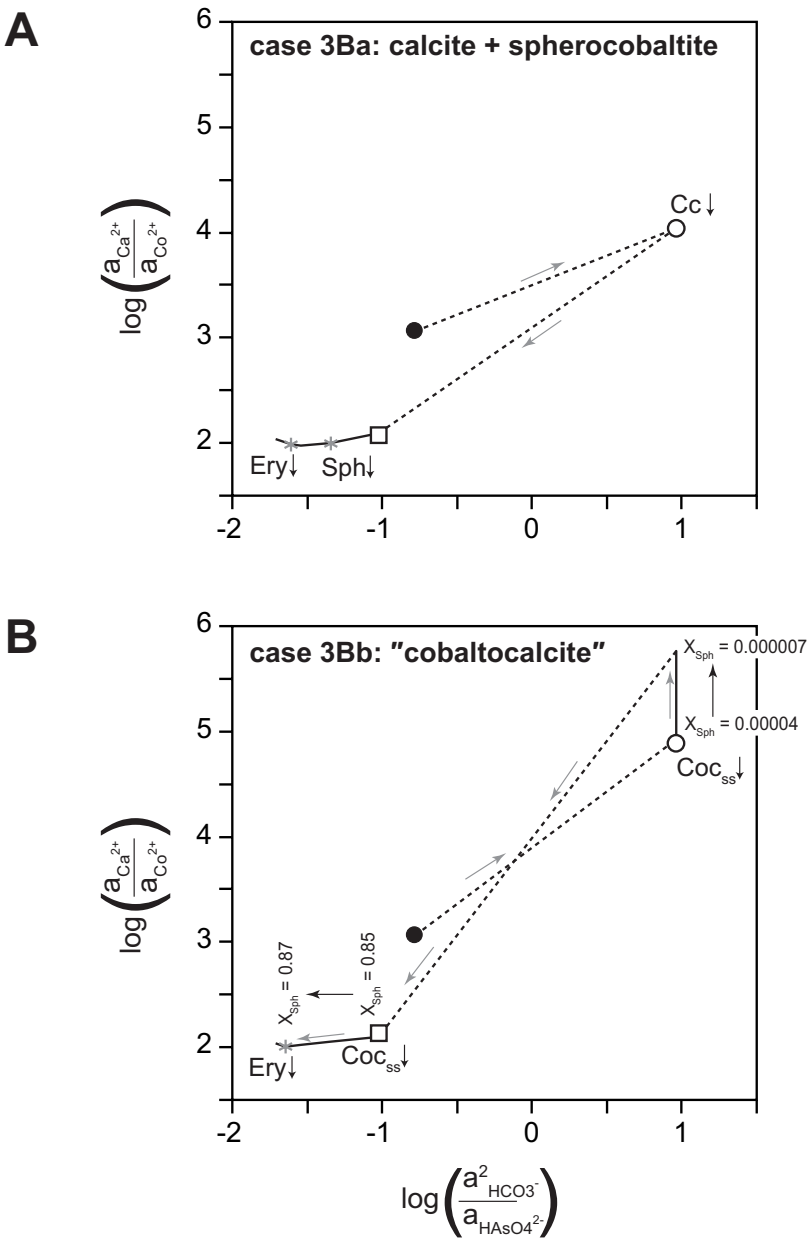
A
case 3Ba: calcite + spherocobaltite
Cc↓
Ery↓
Sph↓
B
case 3Bb: "cobaltocalcite"
X_Sph = 0.000007
X_Sph = 0.00004
Coc_ss↓
X_Sph = 0.87
X_Sph = 0.85
Ery↓
Coc_ss↓
log(a_Ca2+ / a_Co2+)
log(a2_HCO3- / a_HAsO42-)

Figure 14

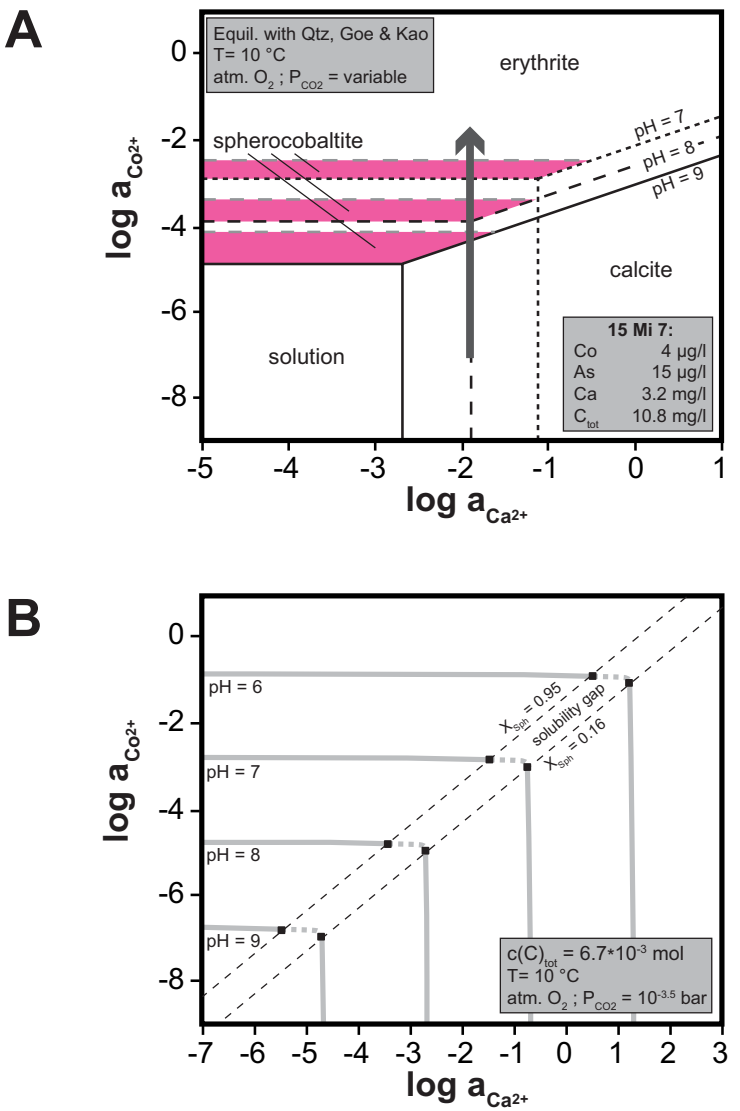
A
Equil. with Qtz, Goe & Kao
T= 10 °C
atm. O2 ; PCO2 = variable
erythrite
spherocobaltite
pH = 7
pH = 8
pH = 9
calcite
solution
15 Mi 7:
Co 4 µg/l
As 15 µg/l
Ca 3.2 mg/l
Ctot 10.8 mg/l
log aCo2+
log aCa2+
B
pH = 6
pH = 7
pH = 8
pH = 9
Xsph = 0.95
solubility gap
Xsph = 0.16
c(C)tot = 6.7*10-3 mol
T= 10 °C
atm. O2 ; PCO2 = 10-3.5 bar
log aCo2+
log aCa2+

Table 1: IMA-approved Ca-Mg-Co arsenates

adelite	$CaMg(AsO_4)(OH)$
brassite	$Mg(AsO_3OH) *4\ H_2O$
camgasite	$CaMg(AsO_4)(OH) * 5\ H_2O$
erythrite	$Co_3(AsO_4)_2 * 8\ H_2O$
ferrarisite	$Ca_5(AsO_3OH)_2(AsO_4)_2 * 9\ H_2O$
guerinite	$Ca_5(AsO_3OH)_2(AsO_4)_2 * 9\ H_2O$
haidingerite	$Ca(AsO_3OH) * H_2O$
hörnesite	$Mg_3(AsO_4)_2 * 8\ H_2O$
irthemite	$Ca_4Mg(AsO_3OH)_2(AsO_4)_2 * 4\ H_2O$
johnbaumite	$Ca_5(AsO_4)_3OH$
pharmacolite	$Ca(AsO_3OH) * 2\ H_2O$
phaunouxite	$Ca_3(AsO_4)_2 * 11\ H_2O$
picropharmacolite	$Ca_4Mg(AsO_3OH)_2(AsO_4)_2 * 11\ H_2O$
rauenthalite	$Ca_3(AsO_4)_2 * 10\ H_2O$
roselite	$Ca_2(Co_{0.8\text{-}0.9},Mg_{0.1\text{-}0.2})(AsO_4)_2 * 2\ H_2O$
rösslerite	$Mg(AsO_3OH) * 7\ H_2O$
sainfeldite	$Ca_5(AsO_3OH)_2(AsO_4)_2 * 4\ H_2O$
talmessite	$Ca_2Mg(AsO_4)_2 * 2\ H_2O$
vladimirite	$Ca_5(AsO_3OH)_2(AsO_4)_2 * 5\ H_2O$
weilite	$Ca(AsO_3OH)$
wendwilsonite	$Ca_2(Mg_{0.8\text{-}0.9}, Co_{0.1\text{-}0.2})(AsO_4)_2 * 2\ H_2O$

Table 2: Ca-Mg arsenate assemblages described and observed from Wittichen (W), St.Marie-aux-Mines, Markirch (M), Richelsdorf (R), Schneeberg (S) and Jachymov, former Joachimsthal (J).

Locality	Assemblage	Reference
W	Hörnesite + pharmacolite	this work
W, R	Hörnesite + weilite	this work, [5]
W	Hörnesite + picropharmacolite	this work, [1]
W, R	Hörnesite + rauenthalite	[1], [5]
W, M, R	Pharmacolite + picropharmacolite	this work, [1], [4], [5]
W, R	Pharmacolite + sainfeldite	this work, [1], [5]
W, M, R	Pharmacolite + weilite	this work, [1], [4], [5], [7]
W	Pharmacolite + guerinite	this work, [1]
W, M	Pharmacolite + ferrarisite	this work, [4]
W, R, S	Sainfeldite + guerinite	this work, [1], [5], [6]
W, R	Sainfeldite + ferrarisite	this work, [5]
W, R	Sainfeldite + picropharmacolite	this work, [1], [5]
W	Sainfeldite + ?wendwilsonite	this work
W, R	Sainfeldite + rauenthalite/phaunouxite	this work, [5]
W, R, S	Guerinite + rauenthalite/phaunouxite	this work, [5], [6]
W, S	Guerinite + picropharmacolite	this work, [1], [6]
W	Picropharmacolite + wendwilsonite	this work
W, M	Picropharmacolit + rauenthalite/phaunouxite	this work, [1], [4]
W	Guerinite + ?roselite	[1]
W, M, R, J	Pharmacolite + haidingerite	[1], [4], [5], [7]
W, J	Rösslerite + ?haidingerite(?)	[1], [7]
W	Picropharmacolite + ferrarisite	[2]
W	Camgasite + hörnesite	[3]
M, J	Picropharmacolite + talmessite	[4], [7]
M, R	Picropharmacolite + ferrarisite	[4], [5]
M	Rösslerite + hörnesite	[4]
M, J	Rösslerite + pharmacolite	[4], [7]
R	Picropharmacolite + weilite	[5]
R	Picropharmacolite + haidingerite	[5]
R	Ferrasite + weilite	[5]
R	Sainfeldite + weilite	[5]
R	Ferrasite + rauenthalite/phaunouxite	[5]
R, J	Rösslerite + picropharmacolite	[5], [7]
R, J	Rösslerite + brassite	[5], [7]

References: [1] = Walenta (1972), [2] = Walenta (1987), [3] = Walenta & Dunn (1989), [4] = Bari (1983), [5] = Schnorrer-Köhler (1983), [6] = Massanek & Michalski (2005), [7] = Hlousek & Trvdy (2002).

Table 3: Localitites, pH-values, TDS, conductivity and concentration data for Ca, Mg, Co, Ni and As of the studied water samples. A full data set for all water samples is provided as an electronic supplement.

sample	locality	in contact with	T [°C]	TDS [mg/l]	conductivity [µS/cm]	pH	Ca [mg/l]	Mg [mg/l]	Co [µg/l]	Ni [µg/l]	As [µg/l]
01Ma	Emanuel, Reinerzau	Granite	12.9	77	157	7.7	21.2	6.5	<0.01	<0.1	3.2
01Mi1		Fluorite			(285)	7.6	41.4	10.5	<0.01	<0.1	5.6
01Mi2		Barite	12.4	123	252	7.7	34.8	13.1	<1	<0.7	35.9
02Mi1	Alte Gaben Gottes, lower adit, Reinerzau	Sinter (white)			(77)	6.3	5.7	0.5	<1	<0.7	1.7
02Mi2		Sinter (brown)			(41)	6.4	2.6	0.3	<1	<0.7	0.9
03Ma	Alte Gaben Gottes, upper adit, Reinerzau	Granite	10.1	15	30	6.6	2.6	0.4	<0.01	<0.1	2.3
03Mi1		Fluorite					19.9		<1	1.3	14.3
04Mi1	Daniel, Wittichen	Barite			(110)	6.5	13.6	3.1	<1	2.5	3.6
05Mi1	Georg, Wittichen	Sinter (white)				7.7	34.1		<1	<0.7	14.5
05Mi2		Granite (strongly altered)			(201)	6.8	28.9	5.3	<0.01	<0.1	8.0
05Mi3		Sinter (white)			(314)	7.3	40.5	13.2	<1	<0.7	20.2
05Mi4		Sinter (white)			(287)	7.0	41.1	10.7	<1	<0.7	39.5
06Ma	Dreikönigstern, Reinerzau	Sinter (black)	10.7	73	148	6.8	23.9	3.9	0.12	<0.1	2.8
07Ma	Johann, Wittichen	Barite	10.3	20	40	6.3	4.6	0.7	0.06	0.40	1.5
07Mi1		Fluorite			(54)	6.5	5.0	0.7	<1	<0.7	1.6
07Mi2		Sinter (darkbrown)			(83)	6.3	10.9	1.2	<1	<0.7	4.0
08Ma	Michael, Schiltach	Granite (strongly altered)	13.6	64	132	7.1	10.3	2.7	0.11	1.1	6.9
08Mi1		Sinter (white)			(336)	7.6	36.4	25.0	<1	<0.7	2.0
08Mi2		Sinter (pinkish-green)			(510)	7.6	69.1	12.7	<1	38.4	74.3
08Mi3		Sinter (brown)			(145)	6.9	15.9	4.9	6.5	11.0	<0.4
09Ma	Hilfe Gottes, Schiltach	Granite (strongly altered)	11.7	85	175	6.9	19.6	8.4	0.05	<0.1	10.5
09Mi1		Barite			(64)	6.8	5.8	1.9	0.13	0.30	5.2
09Mi2		Sinter (brown)			(73)	6.3	6.4	2.1	1.7	<0.7	11.1
10Mi1	Maria Magdalena, Schiltach	Granite (strongly altered)			(58)	6.8	3.9	0.6	<1	<0.7	20.7
10Mi2		Granite (strongly altered)			(59)	6.8	4.1	0.5	<1	<0.7	54.9
11Ma	Güte Gottes, Wittichen	Arkose	12.0	180	371	7.2	39.3	22.4	0.05	<0.1	46.7
12Mi1	Frisch Glück, Wittichen	Granite (strongly altered)			(275)	7.3	38.7	15.0	<0.01	0.79	330
12Mi2		Sinter (black)			(367)	7.6	41.1	9.0	<1	<0.7	2400
12Mi3		Sinter (purple)			(344)	7.6	41.1	9.4	71.5	120	4500
12Mi4		Sinter (multicolored)			(365)	7.6	50.6	20.2	<0.01	<0.1	220
12Mi5		Sinter (purple)			(453)	7.4	48.4	27.8	75.5	240	7500

13Ma	Johann Georg, Wittichen	Granite (casting)	8.8	101	208	7.7	32.0	8.0	0.75	3.5	330
13Mi1		Sinter (purple)			(282)	7.4	30.0	20.0	21.9	36.2	1300
13Mi2		Sinter (purple-green)			(327)	7.6	42.2	17.3	3.8	100	10800
13Mi3		Granite (strongly altered)			(209)	7.4	34.1	5.7	0.17	1.9	160
13Mi4		Granite (strongly altered)			(131)	7.0	19.2	3.5	<0.01	<0.1	16.2
13Mi5		Sinter (white)			(420)	7.6	59.5	18.7	<1	5.0	24.4
13Mi6		Sinter (black)			(277)	7.4	36.2	11.1	<1	<0.7	220
13Mi7		Sinter (darkbrown)			(311)	7.6	41.5	11.7	<1	<0.7	290
14Mi1	Löw-Leostollen, Wittichen	Sinter (brown)			(353)	7.7	38.1	19.8	<1	<0.7	530
14Mi2		Sinter (black)			(351)	7.9	39.2	20.5	<1	<0.7	350
14Mi3		Sinter (white)			(309)	7.6	36.9	17.1	<1	<0.7	220
15Ma	Anton, Heubachtal	Granite (casting)	8.7	72	147	6.8	20.0	7.2	0.05	0.44	18.3
15Mi1		Barite			(194)	7.4	24.9	11.1	<1	<0.7	160
15Mi2		Erythrite			(222)	7.1	27.1	13.0	420	110	2500
15Mi3		Hematite mud			(128)	7.4	16.1	6.0	19.4	9.5	54.8
15Mi4		Green „Ruschel“			(150)	7.4	17.6	7.7	<1	3.1	270
15Mi5		Sinter (darkbrown)			(350)	7.4	50.3	15.0	<1	<0.7	100
15Mi6		Granite	9.5		(133)	7.0	17.2	5.0	<0.01	<0.1	12.4
15Mi7		Granite (altered)			(45)	7.0	3.2	0.7	4.1	<0.7	14.6
16Mi1	Katharina, Heubachtal	Granite (strongly altered)			(103)	6.8	11.7	3.3	<1	<0.7	8.4
16Mi2		Barite			(87)	6.7	9.8	1.5	<0.01	<0.1	3.7
16Mi3		Barite			(187)	7.0	27.5	5.1	<1	2.2	14.6
16Mi4		Granite (altered)			(59)	6.7	6.0	1.4	0.05	0.9	1.2
17Mi1	Hohberg, Hohberg	Fluorite			(40)	6.1	3.1	0.2	<1	<0.7	0.8
17Mi2		Fluorite			(46)	6.2	4.4	0.5	<0.01	<0.1	<0.7
18Ma	Flussspatgrube, Reinerzau	Granite (strongly altered)	10.3	85	175	7.5	24.5	7.0	<0.01	<0.1	24.6
18Mi1		Sinter (brown)			(58)	6.5	6.1	0.9	<0.01	<0.1	16.7
18Mi2		Sinter (brown)			(48)	6.5	4.6	0.7	0.08	<0.1	11.4
18Mi3		Fluorite					9.8		<1	1.9	20.8
18Mi4		Barite			(79)	6.8	8.9	1.1	<1	<0.7	18.1
19Ma	Herzog Friedrich, Reinerzau	Granite (casting)	8.8	148	302	8.3	38.5	18.6	0.51	0.68	250
19Mi1		Sinter (white)			(297)	6.8	39.2	16.4	<1	2.2	230
19Mi2		Granite (altered)			(94)	7.2	10.7	5.0	0.45	0.37	8.9